國 立 中 央 大 學

Physics Department

Master thesis

# VUV and EUV irradiation of $CH_4$+$NH_3$ ice mixtures

研究生: Leung Pui Shan

指導教授: Chen Yu Jung

November 2017

# 國立中央大學圖書館
# 碩博士論文電子檔授權書

(101 年 9 月最新修正版)

本授權書授權本人撰寫之碩/博士學位論文全文電子檔(不包含紙本、詳備註 1 說明)，在「國立中央大學圖書館博碩士論文系統」。(以下請擇一勾選)

(　　)**同意** (立即開放)

(　　)**同意** (請於西元 _____年_____月_____日開放)

(　　)**不同意**，原因是：_____

在國家圖書館「臺灣博碩士論文知識加值系統」

(　　)**同意** (立即開放)

(　　)**同意** (請於西元 _____年_____月_____日開放)

(　　)**不同意**，原因是：_____

以非專屬、無償授權國立中央大學、台灣聯合大學系統圖書館與國家圖書館，基於推動「資源共享、互惠合作」之理念，於回饋社會與學術研究之目的，得不限地域、時間與次數，以紙本、微縮、光碟及其它各種方法將上列論文收錄、重製、與利用，並得將數位化之上列論文與論文電子檔以上載網路方式，提供讀者基於個人非營利性質之線上檢索、閱覽、下載或列印。

研究生簽名: _____　　學號：_____

論文名稱:_____

指導教授姓名：_____

系所 ：_____所　☐博士班　☐碩士班

備註：

1. 本授權書之授權範圍僅限電子檔，紙本論文部分依著作權法第 15 條第 3 款之規定，採推定原則即預設同意圖書館得公開上架閱覽，如您有申請專利或投稿等考量，不同意紙本上架陳列，須另行加填聲明書，詳細說明與紙本聲明書請至 http://thesis.lib.ncu.edu.tw/ 下載。
2. 本授權書請填寫並**親筆**簽名後，裝訂於各紙本論文封面後之次頁（全文電子檔內之授權書簽名，可用電腦打字代替）。
3. 請加印一份單張之授權書，填寫並親筆簽名後，於辦理離校時交圖書館（以統一代轉寄給國家圖書館）。
4. 讀者基於個人非營利性質之線上檢索、閱覽、下載或列印上列論文，應遵守著作權法規定。

# 國立中央大學碩士班研究生

# 論文指導教授推薦書

_____學系/研究所_____研究生所提之論文

_____ 係由本

（題　　目）

人指導撰述，同意提付審查。

指導教授_____ (簽章)

____年____月____日

# 國立中央大學博士班研究生

# 論文口試委員審定書

_____學系/研究所_____研究生所提之論文

_____

經本委員會審議，認定符合博士資格標準。

學位考試委員會召集人 _____

委　　員 _____

_____

_____

_____

中 華 民 國　　年　　月　　日

# Contents

# List of Figures


國立中央大學

# List of Tables


國立中央大學

# 1. Introduction

According to Hindu cosmological mythology, ancient people believe that a giant turtle bears the world on its back. Even after we stepped onto the moon at 1969, there are still plenty that we cannot explain. In the novel Lord of the Rings, the author named the path between hobbits as Mordor, which is also the name of the dark area on Pluto's moon, Charon. Recently, Mission New Horizons retrieved valuable data about Charon and Pluto. This thesis aimed to investigate the chemistry of VUV and EUV irradiations on $CH_4$+$NH_3$ ice mixtures, which is possibly the main compositions to form the red polar cap on Charon in figure 1.1.

According to Infrared (IR) spectroscopy, surface of Charon is a mixture of 90 % $H_2O$ and 10 % tholin at millimetre depth. The main component which forms the dark red cap (tholin) is cold-trapped methane from Pluto's atmosphere ejecta [3]. The second possible component is ammonia. Since ammonia hydrate can be observed by earth-based telescopes [4]. Also in far IR spectrum taken by LEISA camera on the New Horizons, concentrated ammonia is found on Organa crater (figure 1.2) and throughout Charon (figure 1.3) [2]. The third component is methane. The presence of nitrogen and other ejecta from Pluto are neglected in this thesis because according to the model of Hoey et al.[3] (figure 1.4), during New horizons' approach, 98 % of the arrived ejecta is $CH_4$. $CH_4$ remains undetectable by infra-red spectroscopy nor VUV spectroscopy.

Ly-$\alpha$ appears to be the largest source in the dark side of Charon, with attributions from both solar occultation (70 %) and resonance scattering by atomic hydrogen flow (30 %) in the solar system at flux $3.5 \times 10^7$ photons $cm^{-2}$ $s^{-1}$ onto the winter pole of Charon [1]. The flux is 50 % larger than expected before Mission New Horizons [5]. $CH_4$

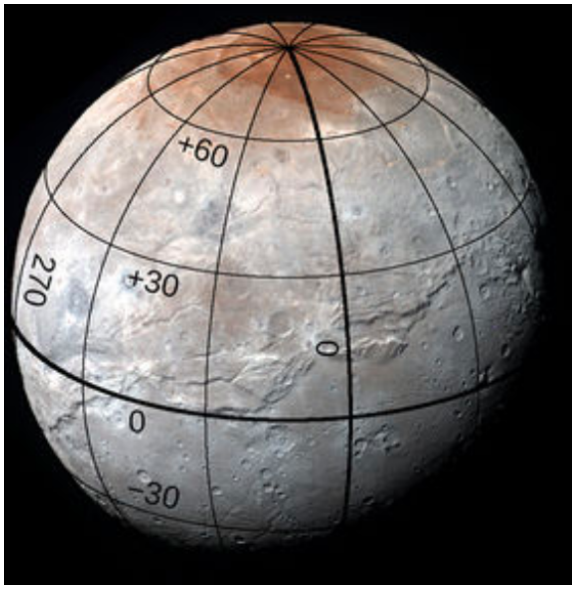


Figure 1.1: An overlapped figure of Charon taken from 3 filters of MVIC camera and LORRI camera to show topological details. (quoted from [1])

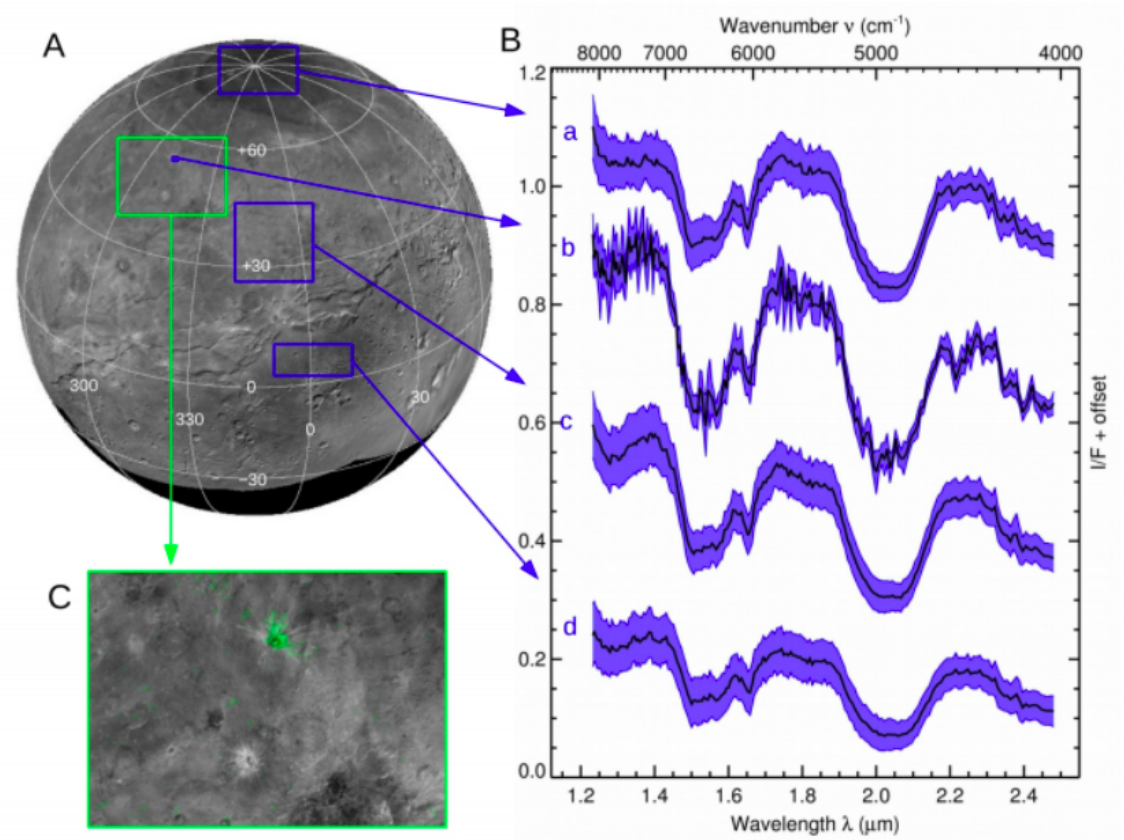


Figure 1.2: The 2.2$\mu$m absorption taken by LEISA camera colored as green on the topology shown by LORRI camera (A) and the spectra at 4 positions with b taken near organa crater.(quoted from [2])

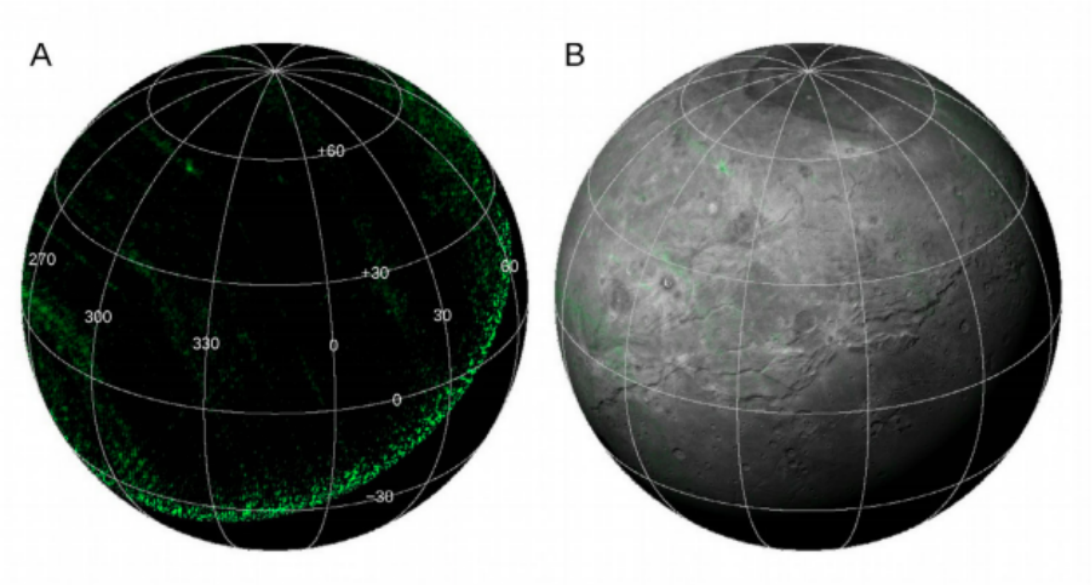


Figure 1.3: The 2.2 $\mu$ m absorption taken by LEISA camera with ammonia marked as green (A) and the topology shown by LORRI camera (B).(quoted from [2])

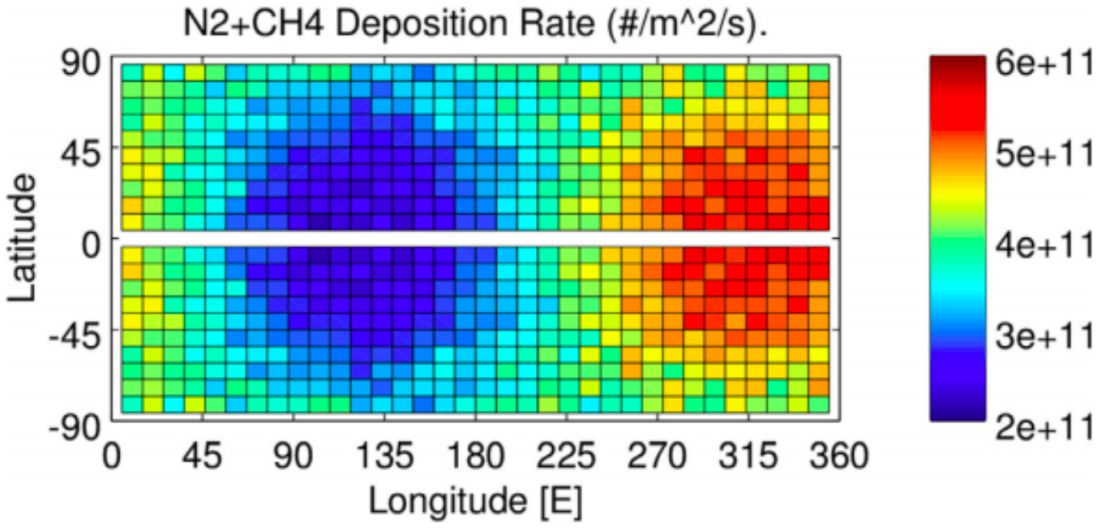


Figure 1.4: The simulation of $N_2$ and $CH_4$ model assuming all arrived molecules will stick onto the surface of Charon. Among the deposition rate, 98 % of them are $CH_4$ because $CH_4$ is lighter and preferentially escapes. The molar fraction of $CH_4$ increase from hypothesized 0.44 % to 42 % in the exobase of Pluto.(quoted from [3])

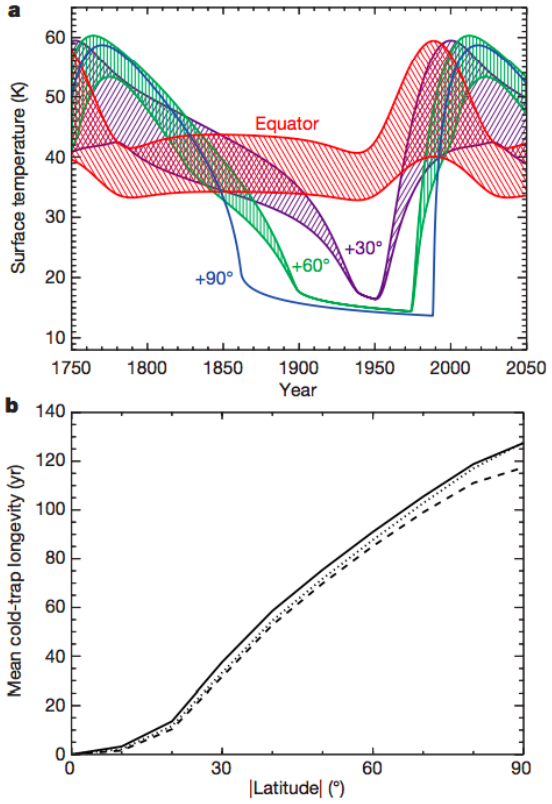


Figure 1.5: The temperature of Charon with thermal inertia 10 J $m^{-2}$ $K^{-1}$ $s^{-1/2}$ in 1750 to 2050 Earth years (a) and longest time the Latitude is under 25 K with the model averaged for 3 Myr with 2.5 (solid) 10 (dotted) and 40 (dashed) J $m^{-2}$ $K^{-1}$ $s^{-1/2}$ (b).(quoted from [1])

deposits at temperature below 25 K at pressure $7.4 \times 10^{-14}$ torr. The time for depositing $CH_4$ is 2 times longer at the pole (130 earth years) than at 45° lattitude according to the thermal model of Grundy et al. [1] (figure 1.5). In order to understand the formation of tholin at different latitudes of Charon, we performed VUV irradiation on $CH_4$+$NH_3$ experiments with different ratios (including 3:2, 1:5, 1:10 and 1:20 for $CH_4$+$NH_3$ to simulate the conditions at different latitudes on Charon with base pressure $3 \times 10^{-10}$ torr, simulating atmosphere on Charon at 15 K, which corresponds to temperature on Charon at winter times [1] in interstellar processing system (IPS) [6].

Apart from VUV irradiation, EUV irradiation also took part. VUV irradiation is believed to be the main process to convert $CH_4$ into heavier molecules which remained on the surface of Charon until the temperature of Charon become 60 K, at which methane evaporates from the ice. The ice is then further processed by EUV, solar wind, coronal mass ejec-

tions and interstellar pickup ions, etc to produce the tholin on Charon [1]. The EUV irradiation (>12.4 eV) is $8.7\times10^{7}$ eV cm$^{-2}$ s$^{-1}$ at mean heliocentric distance 39 A.U. whereas VUV irradiation (Ly-$\alpha$) is $1.9\times10^{9}$ eV cm$^{-2}$ s$^{-1}$[1]. In order to investigate the effectiveness of EUV to VUV irradiation, we kept temperature of $CH_4$+$NH_3$ (3:2 & 1:5) ice mixtures at 15 K and use the monochromatic 30.4 nm (He II) light provided by High flux beamline at National Synchrotron Radiation Research Centre (NSRRC) in Taiwan to irradiate the ice mixtures.

In this text, we will introduce the experimental methodology in chapter 2, theformation reaction mechanisms of $CH_4$+$NH_3$ ice mixtures in EUV and VUV irradiation, a functional group comparison with tholin on Titan will be made in chapter 3. With these results, we will have a better understanding about Charon, different energy sources including electron irradiation experiments , EUV and VUV irradiations, and their astrophysical implications will be presented in chapter 4.


國立中央大學

# 2. Methods

## 2.1 Laboratory Astrophysics

To study the chemical reactivity in astrophysical environment experimentally, we conducted our experiments in Interstellar photoprocessing system (IPS) [6], an ultrahigh vacuum chamber with base pressure $3 \times 10^{-10}$ torr and 14 K, corresponds to a density of $10^6$ cm$^{-3}$, similar to dense cloud interiors. The system will be introduced in detail in section 2.1.1. To simulate the irradiation in interstellar environments, we use a micro-wave discharge hydrogen lamp (MDHL) and monochromatic extreme-ultraviolet irradiation (EUV) 30.4 nm to irradiate our ice mixtures, and they will be introduced in section 2.1.2 and 2.1.3 respectively. The experimental protocols will be elaborated in section 2.2. In order to better understand the physics behind, some basic theories of Infrared spectroscopy and concepts of chemical kinetics used in data analysis are included in section 2.3 and 2.4 respectively.

### 2.1.1 Experimental simulations by IPS system

We conducted our astrophysical simulations in Interstellar Photo Processing System (IPS) (figure 2.1). IPS consists in three systems: the main chamber, where our experiments take places; the detection system, where we collect our data; and a gasline system, where we prepare our samples.

The main system consists of an ultrahigh vacuum chamber equipped with a closed-cycle helium cryostat (CTI-M350). It is pumped by a turbo molecular pump, which is backed up by a scroll pump, and a non –evaporation getter pump. The getter pump is a powerful tool to adsorb residue gases inside the main chamber, with a larger surface area, $H_2$, CO and $N_2$ are adsorbed to obtain a better base pressure. After baking,

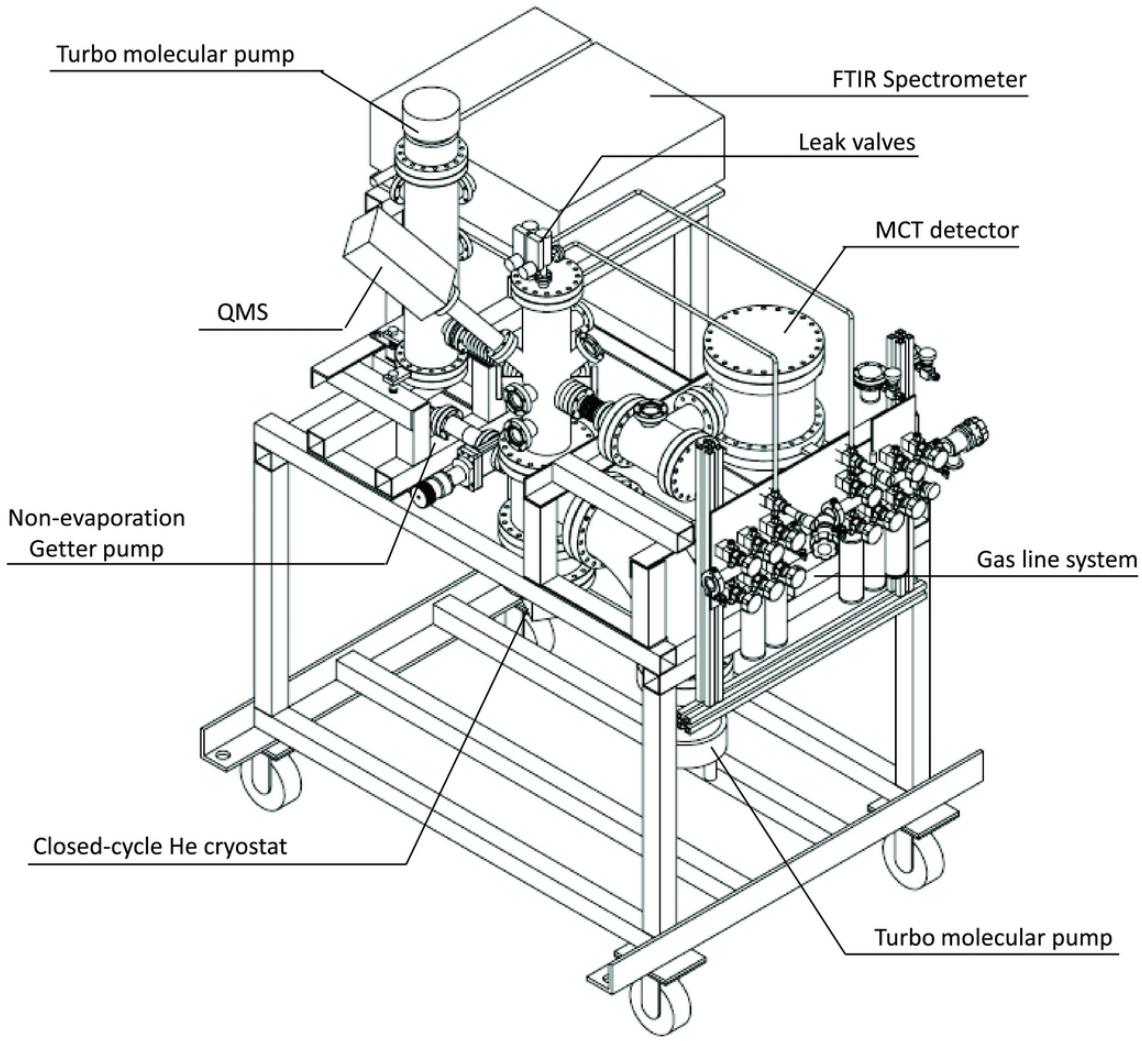


Figure 2.1: The schematic diagram of IPS system, mechanical pumps are not shown for clarity. (Quoted from Chen et al. 2014)

the base pressure of our main chamber can reach $1 \times 10^{-10}$ torr at 14 K, monitored by a Granville-Phillips 370 Stabil-Ion gauge. This pressure can be used to demonstrate the dense cloud interior environments and star forming region. The substrate we have chosen is KBr, which can allow infra-red photons with 700 to 4000 $cm^{-1}$ to penetrate. It is mounted by substrate holder made of oxygen-free copper, on the second stage of cold finger mounted on the tip of cryostat. Two silicon diodes and also a heater were placed onto the cold finger and one of the silicon diodes is near the substrate holder. They were connected to a temperature controller and PID system to achieve a warmup rate of 1K/min with an accuracy of 0.1 K.

The detection system consists in a mid-infrared Fourier transform spectrometer (mid-FTIR) (ABB FTLA2000-104) and a Quadrupole Mass Spectrometer (QMS). To prevent absorption bands of CO, $CO_2$ and $H_2O$ gas in the atmosphere, the IR beam path was built inside vacuum, pumped by dry pump. The main chamber and the IR path are separated by ZnSe windows, which can allow infra-red penetration from 0.5 – 20 um with absorption less than 0.07 %. In this study, the infrared spectra are obtained with resolution of 4 $cm^{-1}$ and averaged over 32 scans. The angle between the IR beam path and the substrate holder is 45 degrees. The QMS (MKS Microvision 2) consists of a controller and mechanical part sealed by a mounting flange in ultrahigh vacuum. It is mounted 10 cm from the substrate and run with a resolution 0.5 a.m.u. The Ionizer release 70 eV electron by filament and ionize incoming molecules to positive charged ions between anode grid and repeller. The ions were accelerated by focus plate and enters ion filter, which consists of four circular rods, with a combination of A.C and D.C. potential to sieve whole bandpass ions at millisecond timescale. The selected ions enter ion detector and are detected by either faraday cup and continuous dynode electron multiplier (CDEM) which can secondary multiply weak signals.

The samples are prepared in situ in our gasline system. It contains four stainless steel bottles with the same volume, which is used to determine relative proportion of the gas mixtures by their partial

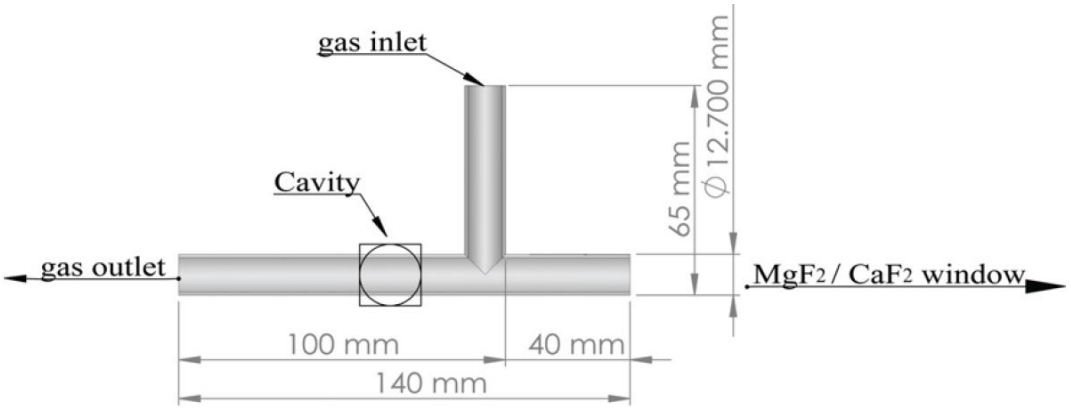


Figure 2.2: The cross-section of MDHL (T-type geometry) (Quoted from Chen et al. 2014).

pressures. The ammonia gas 99.99 % and methane 99.999 % are mixed with partial pressure measured by a Baratron with 0 - 100 torr range with a 0.25% accuracy. The background pressure of the gasline system is lower than $1 \times 10^{-7}$ torr thank to a turbo molecular pump (Oerlikon Leybold TurboVac 151, capacity 145 liters s-1) backed up with an oil-sealed mechanical pump (Alcatel 2012A, capacity 450 $liters minute^{-1}$), equipped with an oil trap (molecular sieve type 13X). Water were bought from Merck which is LC-MS Grade and purified before use, by several freeze-pump-thaw cycles under vacuum.

### 2.1.2 Vacuum-UV source

In order to simulate the photoprocessing of vacuum ultraviolet (VUV) irradiation onto the interstellar ices and ices on planetary bodies, including KBOs, the ice mixtures are irradiated with a T-type Microwave-Discharged Hydrogen-flow lamp (MDHL). The molecular hydrogen with pressure 0.4 torr flows through the lamp with a support of a mechanical pump. Using a 2.4 GHz microwave generator and high voltage discharge, a low pressure plasma is produced in the Evenson cavity. Figure 2.2 shows a cross-section of T-type quartz tube; the middle part of the T-type quartz tube is being tunned by a ceramic rod that is called Evenson cavity. In order to measure the photon flux in situ, we use an 88 % transmittance nickel mesh with its photoelectric efficiency being obtained by high-flux beamline in National Synchrotron and a SXUV 100 photodiode calibrated by NIST. A $MgF_2$ window is

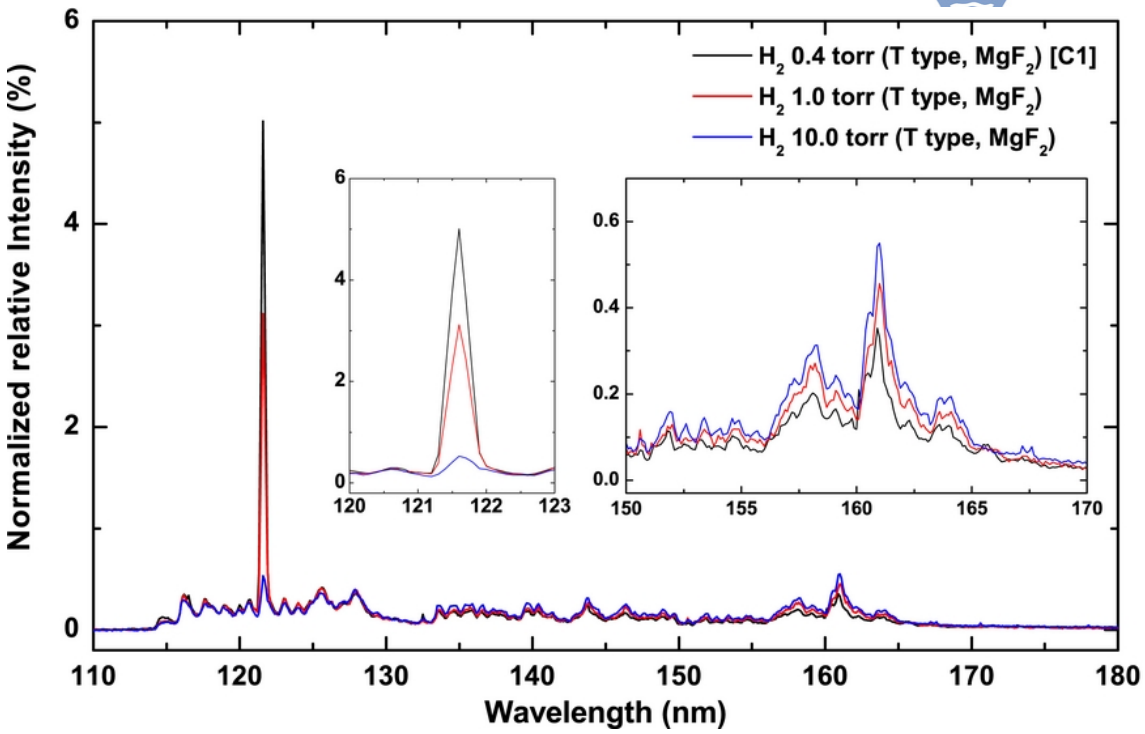


Figure 2.3: VUV spectra of MDHL (T-type geometry, 110-180 nm) with different $H_2$ pressure inside the lamp(Quoted from Chen et al. 2014).

placed between the lamp and the sample holder to prevent penetration of VUV photons with wavelength shorter than 114nm, leads to a cut off at 114nm. Figure 2.3 shows a VUV emission spectrum of a MDHL. It consists in Ly-$\alpha$ (121.6nm) and $H_2$ molecular emission in 110-180 nm range. Chen et al. (2014) showed that the spectral characteristics of the VUV light emitted in this range depends on the gas type (mixture of $H_2$ with He or Ar etc), pressure of $H_2$ and lamp geometry. Throughout those configurations stated there, we adopted 0.4 torr molecular hydrogen and T-type MDHL that produces VUV irradiation at 114-170 nm with 19.1 % of Ly-$\alpha$ and a mean photon energy of 9.27 eV. The photon flux is $6.4 \times 10^{13}$ photons $cm^{-2}s^{-1}$ at sample position.

### 2.1.3 Extreme EUV source

To simulate the solar EUV irradiation reflected by IPM on both Charon and interstellar ices, we use the HF-CGM high – flux beam line of the National Synchrotron Radiation Research Center in Hsinchu, Taiwan. It provides a continuum EUV to VUV photons from 4 to 40 eV. The continuum is separated into monochromatic 30.4nm photons with

a six-meter cylindrical grating monochrometer with an incident angle of 70 degrees. With the help of a movable entrance slit and movable curved exit slit, the energy resolving power can reach around $3 \times 10^4$ at 40 eV for grating 1600 l/mm with both slits movable and set opening to 10 $\mu m$ [7]. Similar to VUV irradiation provided by MDHL, the light intensity was monitored by the same nickel mesh with photoelectric efficiency obtained by SXUV 100 photodiode calibrated by NIST. With the known photoelectric efficiency, the flux of monochromatic 30.4nm is measured to be $2.15 \times 10^{14}$ photons $s^{-1}cm^{-2}$ with a spot size of 1 cm

## 2.2 Experimental Protocol

In this section, we will briefly introduce the procedures of how we performed our experiments. It is divided into four parts, preparation and cooling, deposition, irradiation and warmup.

Preparation of experiments and cooling

Before any of experiment is done, we bake our system at 100 oC for 48 hours to reduce the contamination of water and residue gases as much as possible. It was cooled to room temperature that the background pressure can reach routinely at $1 \times 10^{-10}$ torr. The gasline were connected with the regulators of the gas tanks and bake to 100 $^oC$ and pumped by moleculartur bo pump for two days before any experiment were done. Also, The water sample has been freeze thaw several times by liquid nitrogen until there is no pressure increase recorded by baratron when water is freezed. Before cooling the substrate to cryogenic temperature, we took an IR spectrum and started the monitoring of residue gases by QMS in order to compare the residue molecules and to verify any possible contaminations in the main chamber. We then start the cooling process thanks to the closed-cycle He cryostat.

Deposition

The gas mixtures are pre-mixed in our gasline system introduced in section 2.1.1. We used a leak valve to condense the gas from the stainless steel bottles onto pre-cooled KBr substrate at 14 K, which monitored by Fourier transformed Infra-red spectroscopy (FTIR) and

Quadrupole mass spectrometer (QMS) during deposition. The pressure of deposition is fixed to $1 \times 10^{-8}$ torr that the deposition rate is $4 \times 10^{16} molecules cm^{-2} min^{-1}$. After deposition, we placed the ice mixture at 14 K for 60 minutes and to allow pumping of residue gas, until pressure of the main chamber reduce back to its base pressure to simulate the interstellar environment before irradiation.

Photon Irradiation

The total irradiation time is 270 to 450 minutes depend on experiment configurations; with time intervals varies from 2 to 30 minutes. After each irradiation, we waited for 10 minutes allowing pumping out of the photodesorpted gas molecules. During irradiation, the photon flux is monitored by a nickel mesh. After Irradiation, we place the sample for 30 minutes to observe if any thermal reaction was conducted.

Warmup

We use 1 K/min to warmup the substrate to 300 K to demonstrate effects of a new born star nearby an interstellar cloud. During warmup, we record the QMS from 1 to 100 a.m.u. to observe if there are low quantity of higher mass product formed during irradiation.

## 2.3 Infra-red spectroscopy and the Beer's Law

We used infra-red spectroscopy extensively in chapter 3 and 4, it is a powerful tool in studying molecular interactions during irradiation and warmup. We choose infra-red rather than Ramen spectroscopy because infra-red has lower energy that it would not change the structure of the ice mixture nor breaking any of the bonds. With different vibration modes, the energy absorbed by molecules are quantized. With the energy of absorption bands in infra-red spectrum, we may identify the functional group of the species. To simply classify, molecules can have, from less energetic, translational, rotational and vibrational motions. Generally, vibrational motions can be divided into stretching and bending. Stretching needs more energy than bending. For stretching, there exist Symmetric and Asymmetric stretching, while bending can be

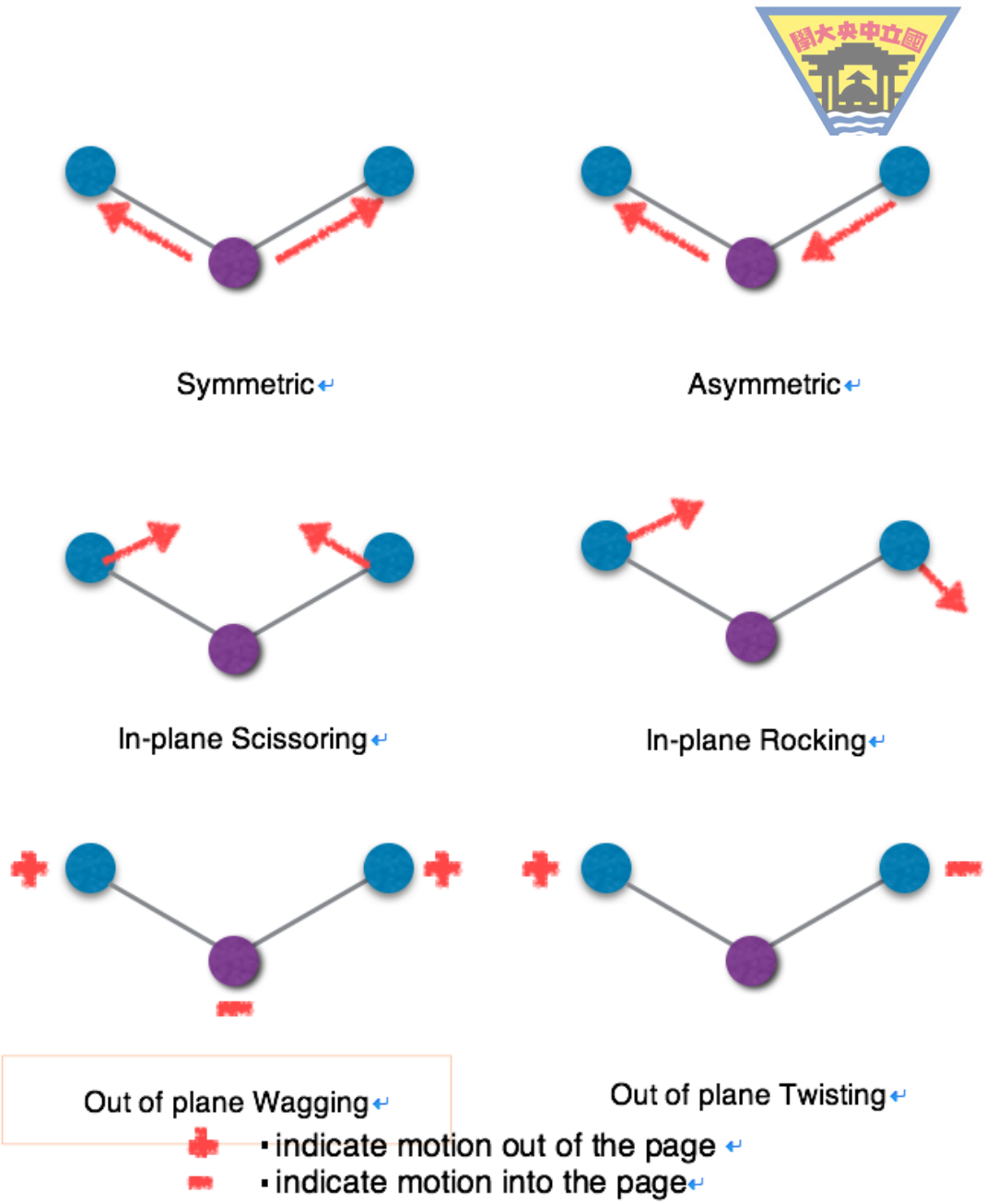


Figure 2.4: Different vibrational modes of a three atom molecule.

divided into In-plane Scissoring, rocking and out of plane Wagging and Twisting (Figure 2.4).

By Beer's Law, we may calculate the column density of the molecule with its functional groups, which are used to plot figures in chapter 3 and 4. Beer Lambert's Law suggest that when light passes through a medium, amount of light absorbed is proportional to density and path length of the medium. Assume the known intensity beam $I_0(\nu)$ passes through the medium and beam intensity become $I(\nu)$. The transmittance $T(\nu)$ is defined by equation 2.1.

$$T(\nu) = \frac{I(\nu)}{I_0(\nu)} \tag{2.1}$$

Also, the absorbance $a(\nu)$ is defined by equation 2.2.

$$a(\nu) = -\ln T(\nu) = -\ln \frac{I(\nu)}{I_0(\nu)} = nl\sigma(\nu) \tag{2.2}$$

where $n$ is number density (molecules/cm$^3$), $l$ is the path length (cm), $\sigma(\nu)$ is the cross-section (cm$^2$/molecule) of corresponding frequency $\nu$. This equation is known as Lambert Beer's Law.

As the ice mixture in our thesis are at 14K, the peaks of absorbance are often a broadband due to coupling between neighbor molecules. Therefore, we can integrate the whole band of the peak equation 2.2 with respect to frequency and use the absorbance strength (A value) in literatures to calculate the column densities $N$ of the ices by equation 2.3.

$$N = \frac{\int a(\nu)\mathrm{d}\nu}{A(\nu)} \tag{2.3}$$

where $N$ is the column density (molecule cm$^{-2}$), $A(\nu)$ is the absorbance strength (cm molecule$^{-1}$).

## 2.4 Reaction Rate Laws

In this section, we will introduce rate reaction of a consecutive reaction and the concept of pseudo first order which we used to fit our reaction product against irradiation time. The rate of a chemical reaction is the relation between change in concentration of a substance per unit of time. i.e. For a balanced chemical reaction, A $\rightarrow$ 2B, the rate of reaction is $-\frac{\Delta[A]}{\Delta t}$. The formation rate of B is 2 times destruction rate of A.

To determine the order of a reaction, we can only determine it experimentally. For a zero order reaction, the rate is not depending on any reactant that it is a constant. The rate $= -\frac{\Delta[R]}{\Delta t} = k[R]^0$. By calculus, $[R]_0 - [R]_t = kt$.

For a first order reaction, rate $= -\frac{\Delta[R]}{\Delta t} = k[R]$. By calculus, $\ln[R]_t = -kt + \ln[R]_0$.

For a second order reaction, rate $= -\frac{\Delta[R]}{\Delta t} = k[R]^2$. By calculus, $\frac{1}{[R]_t} - \frac{1}{[R]_0} = kt$.

Hence, if we get a straight line in a time versus concentration plot ,it is a zeroth order reaction, similarly, in first order reactions, we get proportional relationships in time versus $\ln[R]$.

In a reaction with one reactant in excess, the rate of reaction is called pseudo first order reaction where pseudo means pretended. For A+B $\rightarrow$ C, rate $= k[A][B]$. As $[B]_0 \gg [A]_0$, change of $[B]$ is negligible that $[B] \sim [B]_0$. Therefore, $[B]$ is assumed to be a constant and included in the rate constant k.

For a consecutive reaction equation, which we used to fit our data points, where A $\rightarrow$ B $\rightarrow$ C that the produced product will not convert back as reactant. A simple example is radioactive decay. At $t = 0$, $[A] = [A]_0$, $[B] = 0$, $[C] = 0$ and at all times, $[A] + [B] + [C] = [A]_0$. The rate equations are as follows:

$$-\frac{\Delta[A]}{\Delta t} = k_1[A] \tag{2.4}$$

$$-\frac{\Delta[B]}{\Delta t} = k_1[A] - k_2[B] \tag{2.5}$$

$$-\frac{\Delta[C]}{\Delta t} = k_2[B] \tag{2.6}$$

By equation 2.4, we get

$$[A] = [A]_0 e^{-k_1 t} \tag{2.7}$$

By substituting equation 2.7 into equation 2.5, we get

$$-\frac{\Delta[B]}{\Delta t} + k_2[B] = k_1[A]_0 e^{-k_1 t} \tag{2.8}$$

After solving the differential equation 2.8 , we get

$$[B] = \frac{k_1}{k_2 - k_1}(e^{-k_1 t} - e^{-k_2 t})[A]_0 \tag{2.9}$$

Finally, since $[C] = [A]_0 - [B] - [A]$, by equation 2.7 and 2.9, we get

$$[C] = \left(1 + \frac{k_1 e^{-k_2 t} - k_2 e^{-k_1 t}}{k_2 - k_1}\right)[A]_0 \tag{2.10}$$


國立中央大學

# 3. Results and Discussions

According to the New Horizons team [1], $CH_4$ from Pluto may accumulate by cold-trapping, onto the surface of Charon. The amount of $CH_4$ varies along the surface of Charon because it depends on the length of time the temperature is below 25 K which in turns depends on diurnal motion and thermal inertia of Charon. With an axis tilted by 112 degrees from the ecliptic, higher concentration of $CH_4$ will be accumulated at the pole (see chapter 1 for details). In this chapter, we will investigate the following by infra-red spectroscopy: 1. The photo products produced by different concentration ratios of methane to ammonia, 2. the photo products produced by different photo sources (i.e. EUV and VUV) 3. the reaction mechanisms of each main products and 4. the functional group of tholin formed by irradiation of VUV, EUV on different configurations of $CH_4$+$NH_3$ ice mixtures (the result is compared with the residues on Titan produced by Imanaka et al. [8]).

## 3.1 The infra-red spectrums and peaks identification

We scanned the IR spectrum before and after deposition and plotted the plot the corresponding absorbance of the ice mixtures. Figure 3.1 is a plot of the absorbance of the $CH_4$+$NH_3$ ice mixtures in different concentration ratios: 1:20, 1:10, 1:5 and 3:2 ( arrangedfrom top to bottom). We labelled the peaks used in column density calculation by dotted lines in the graph. Main products we have detected are $C_2H_6$, $CN^-$ and $C_3H_8$. The peak positions for substance identification are listed in Table 3.1. After identification of the products, we will look into each main products individually.

To calculate the column density, we integrate the area under graph and divided by the absorption strength presented in table 3.2. We aware

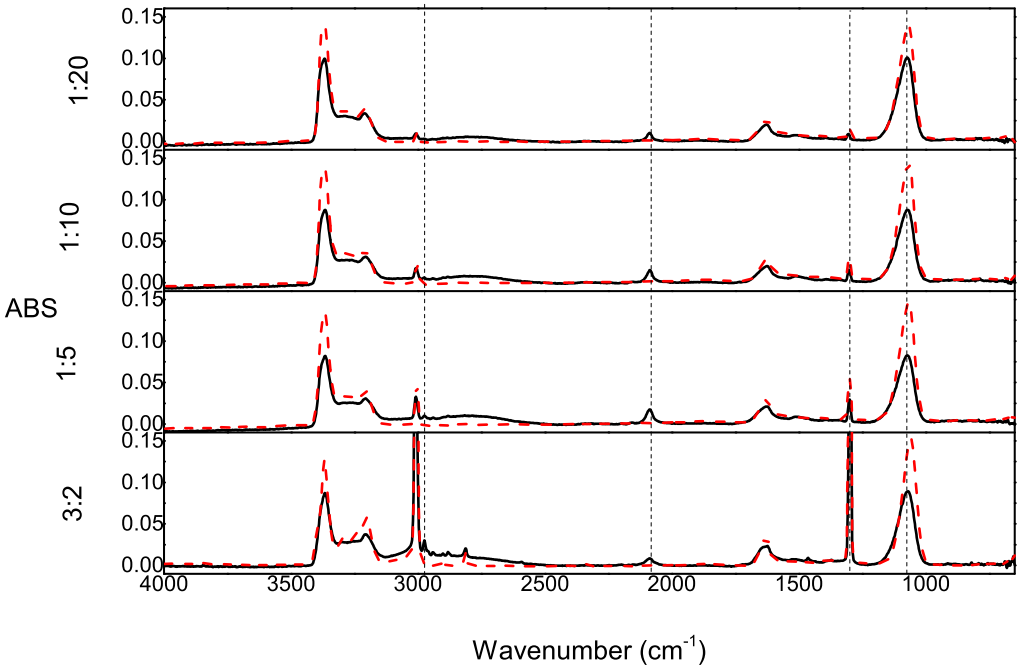


Figure 3.1: The the infra-red spectrum of $CH_4$ + $NH_3$ ice mixtures before irradiation (dashed) and VUV irradiated ice mixtures provided by MDHL.

Table 3.1: The peak positions of identified substances after irradiation in different configurations of ice mixtures.

| Literture assignments | | $CH_4$+$NH_3$ ratio (MDHL) | | | | |
|---|---|---|---|---|---|---|
| Wavenumber ($cm^{-1}$) | Carrier | 1:5 ($cm^{-1}$) | 1:10 ($cm^{-1}$) | 1:20 ($cm^{-1}$) | 3:2 ($cm^{-1}$) | Ref. |
| 3375 | $\nu_3$ ($NH_3$) | 3366 | 3366 | 3369 | 3367 | 1 |
| 3290 | $2\nu_4$ ($NH_3$) | - | - | - | - | 1 |
| 3210 | $\nu_1$ ($NH_3$) | 3207 | 3208 | 3210 | 3205 | 1 |
| 3011 | $\nu_3$ ($CH_4$) | - | - | - | - | 2 |
| 2972 | $\nu_{10}$ ($C_2H_6$) | 2975 | - | - | 2975 | 3 |
| 2960 | $C_3H_8$ | - | - | - | 2960 | 7 |
| 2941 | $\nu_8 + \nu_1 1$ ($C_2H_6$) | 2940 | - | - | 2940 | 3 |
| 2904 | $\nu_1$ ($CH_4$) | 2901 | - | - | 2901 | 5 |
| 2879 | $\nu_5$ ($C_2H_6$) | 2882 | 2883 | - | 2882 | 3 |
| 2814 | $\nu_2 + \nu_4$ ($CH_4$) | - | - | - | 2815 | 5 |
| 2083 | $\nu$ ($CN^-$) | 2088 | 2087 | 2088 | 2088 | 2 |
| 1625 | $\nu_4$ ($NH_3$) | 1625 | 1625 | 1626 | 1631 | 1 |
| 1514 | $\delta$ ($NH_2$) | 1509 | 1507 | 1505 | 1511 | 6 |
| 1465-1440 | deform $CH_2$ scissor | 1461 | - | - | 1463 | 3,4 |
| 1390-1370 | $CH_3$ sym deform | 1394 | 1394 | 1394 | 1372 | 4 |
| 1298 | $\nu_4$ ($CH_4$) | 1301 | 1302 | 1305 | 1299 | 2 |
| 1075 | $\nu_2$ ($NH_3$) | 1073 | 1072 | 1072 | 1072 | 1 |
| 820 | $\nu_1 2$ ($C_2H_6$) | - | - | - | 820 | 3 |

Reference: 1. Bossa et al. 2008 [9] 2. Moore and Hudson 2003 [10] 3. Kim et al. 2010 [11] 4. Socrates 2001 [12] 5. Bennet and Kaiser 2007 [13] 6. Zheng et al. 2008 [14] 7. Hudson and Moore 2004 [15]

that there is an average error in absorption strengths of no more than 10 % when the pure ice is diluted in $N_2$ and $H_2O$ [16]. In our case, absorption strengths changes after $CH_4$ and $NH_3$ are mixed. For example, according to d' Hendecourt and Allamandola [17], the band of $NH_3$ located at 1070 $cm^{-1}$ would not change much (from $1.1 \times 10^{-17}$ to $1.2 \times 10^{-17}$) when excess water is added to pure $NH_3$. For the case of $CN^-$, we know that $CN^-$ has a bond order =3 from its molecular orbitals. $CN^-$ which is different from CN (bond order 2.5). CN stretching is very sensitive to the matrix environment. It can change by factor of 2 in amino acetonitrile and $H_2O$ (1:3) [18]. However, CN is not inspected in this chapter. Therefore, we are justified to use the same absorption strength throughout our discussion to estimate the column density of each species and how the absorption area changes with concentration ratios of ice mixtures and photon energy. Here, we adopt the absorption strengths stated in Table 3.2

Table 3.2: The strength of absorbance adopted in this thesis measured in literatures of pure ice samples

| Wavenumber ($cm^{-1}$) | Assignment | Vibration | FWHM | A value ($\times 10^{-17}$) | Reference |
|---|---|---|---|---|---|
| 2976 | $C_2H_6$ | $-CH_3$ | - | 1.05 | 2 |
| 2960 | $C_3H_8$ | $-CH_2-$ | - | 2.58 | 2 |
| 2086 | $CN^-$ | CN | - | 1.8 | 3 |
| 1297 | $CH_4$ | CH deformation | 8 | 0.61 | 1 |
| 1070 | $NH_3$ | "umbrella mode" | 68 | 1.7 | 1 |

Reference: 1. d'Hendecourt and Allamandola (1986)[17] 2. Moore and Hudson (1998)[19] 3. Noble et al. (2013) [20]

## 3.2 Reaction mechanisms

### 3.2.1 $C_2H_6$

The assignment of $C_2H_6$ is confirmed by several bands listed in table 3.1. Figure 3.2 is a zoomed view of figure 3.1. The absorption peak located at 2075 $cm^{-1}$ corresponds to the strongest vibration of $C_2H_6$. The formation of $C_2H_6$ in astrophysical environment is mainly through a combination with 2 $CH_3$ radicals [21]:

$$CH_4 + h\nu \rightarrow CH_3 \tag{3.1}$$

$$2CH_3 \rightarrow C_2H_6 \tag{3.2}$$

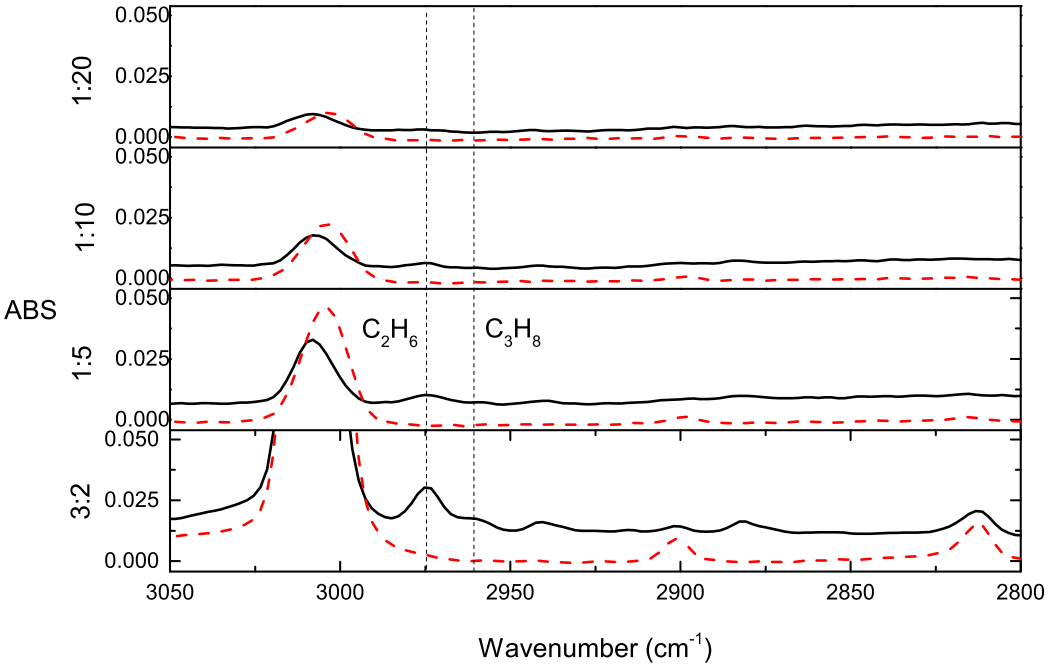


Figure 3.2: The the infra-red spectrum of $CH_4$ + $NH_3$ ice mixtures of $C_2H_6$ and $C_3H_8$ before irradiation (dashed) and VUV irradiated ice mixtures provided by MDHL.

The energy required to produce 1 $CH_3$ radical from $CH_4$ is 4.42 eV. Recombination of 2 $CH_3$ radicals to form $C_2H_6$ releases 3.74 eV. The process in 3.2 is a no-barrier exothermic process. Note that $C_2H_6$ is not detected in $CH_4$ to $NH_3$=1:20 ice mixtures. Figure 3.3 shows the temporal formation column density of $C_2H_6$ in different configurations of irradiated ice mixtures. As the formation only depends on $CH_4$, we may use first order kinetics equation to fit the column density versus photon dose.

$$[A] = [A]_0(1 - e^{-k_1 t}) \tag{3.3}$$

The fitting results are shown in table 3.3.

Table 3.3: The fitting results of $C_2H_6$ by $[C_2H_6]=[C_2H_6](1 - e^{-k_1 t})$

| Ratio of $CH_4$+$NH_3$ | A (x$10^{15}$ molecules cm$^{-2}$) | k (x$10^{-17}$ photon$^{-1}$) |
|---|---|---|
| 1:10 | 2.90 ± 1.25 | 0.92 ± 0.15 |
| 1:5 | 4.16 ± 0.28 | 2.28 ± 0.28 |
| 3:2 | 19.2 ± 0.15 | 5.28 ± 0.25 |

From table 3.3, the production rate is nearly proportional to the

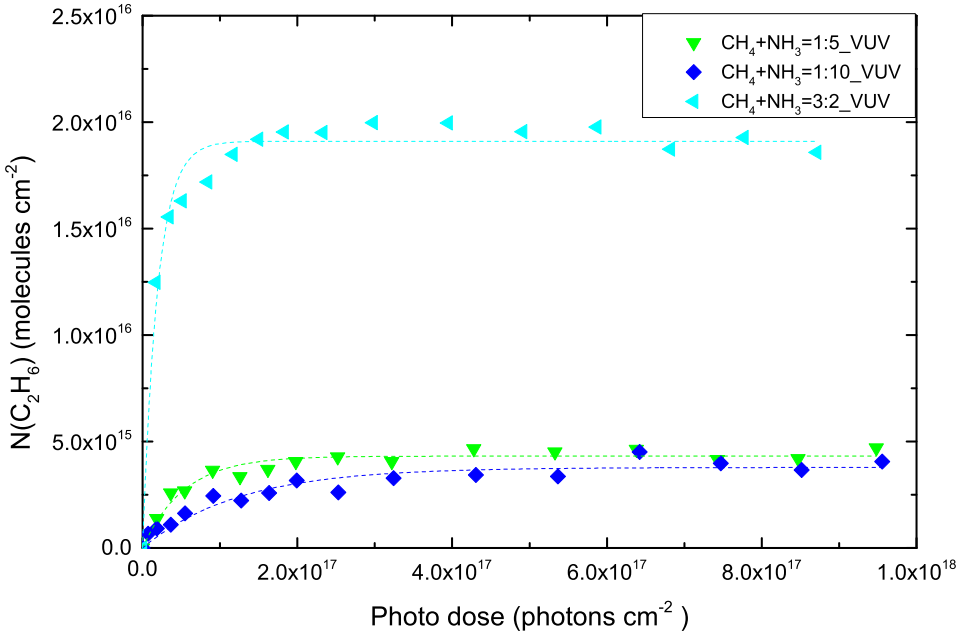


Figure 3.3: The column density of C2H6 during CH4 + NH3 ice mixtures irradiated by MDHL.

initial $CH_4$ concentration.

### 3.2.2 $C_3H_8$

The peak positioned at 2960 $cm^{-1}$ belongs to –$CH_2$- so we assigned that as $C_3H_8$, as the shortest carbon chain. The signal to noise ratio in $CH_4$+$NH_3$ = 1:10 is poor that we can not quantize the amount of $C_3H_8$ (figure 3.2).

It is a secondary product formed by a combination of either $C_2H_6$ + $CH_2$ (equation 3.4)or $C_2H_4$ + $CH_4$ (equation 3.5).

$$C_2H_6 + CH_2 \rightarrow C_3H_8 \tag{3.4}$$

$$C_2H_4 + CH_4 \rightarrow C_3H_8 \tag{3.5}$$

By modern peak fitting method, we deconvoluted the overlapped $C_2H_6$ and $C_3H_8$ into two gaussians.

### 3.2.3 $CN^-$

From infra-red absorption spectrum (figure 3.4) and their positions, we assigned the peak 2086 $cm^{-1}$ to $CN^-$ but not a combination of HCN and $CN^-$. The assignment is based on a absence in CN bending mode at

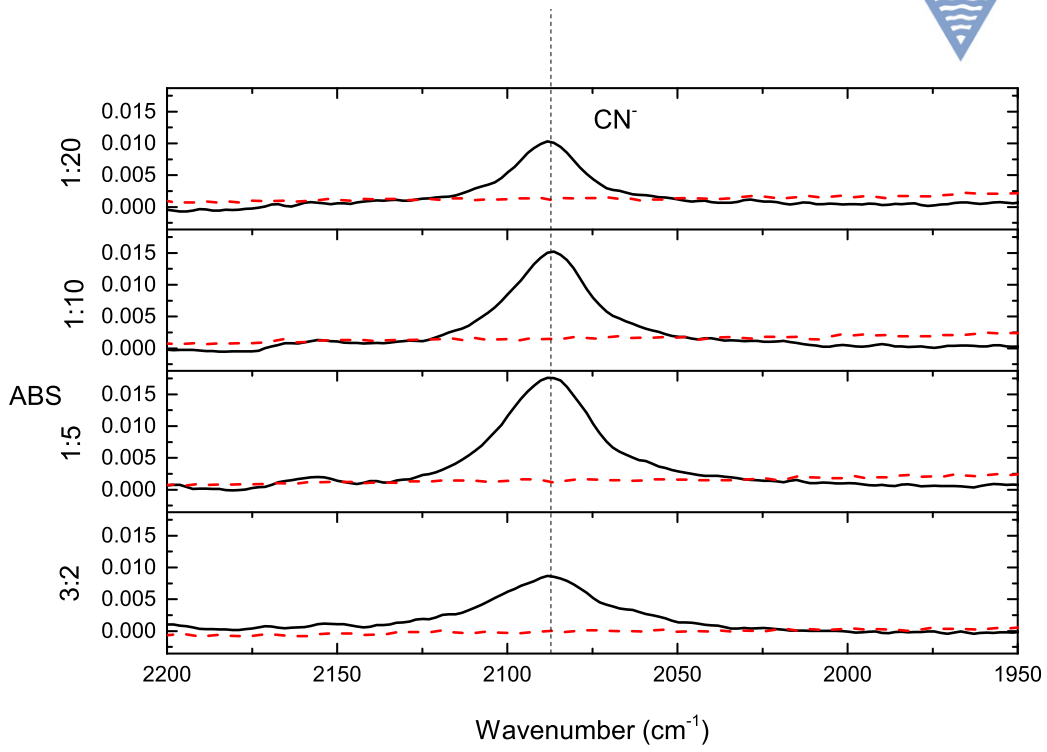


Figure 3.4: The infra-red spectrum of $CH_4 + NH_3$ ice mixtures of $C_2H_6$ and $C_3H_8$ before irradiation (dashed) and VUV irradiated ice mixtures provided by MDHL.

848 $cm^{-1}$. In the case $CH_4 + NH_3 = 3{:}2$, we may observe a peak located at 820 $cm^{-1}$, which is with a FWHM half of HCN and it is eliminated at 50 K during the warm-up phase. Since 50 K is the desorbing temperature of $C_2H_6$ and the peak position is the close to v12 mode of $C_2H_6$, we believe that the 820 $cm^{-1}$ peak is contributed by $C_2H_6$. Therefore, we may assign our peak located at 2086 $cm^{-1}$ as purely $CN^-$.

The formation mechanism of $CN^-$ at low temperature was first suggested by Kim and Kaiser [22] to be two step reaction mechanism with methylamine as intermediate. $CH_4$ and $NH_3$ irradiated by photon to become $CH_3$ and $NH_2$ radical (figure 3.5, followed by propagation and recombination of radicals becoming $CH_3NH_2$ and dehydrogenation and acid-base reaction to form $CN^-$. Although Kim and Kaiser [22] used 1.5 keV electron as energy source to simulate the cosmic ray induced photochemistry, this formation mechanism also applies in our photon irradiation experiments because we can also detect the methylamine

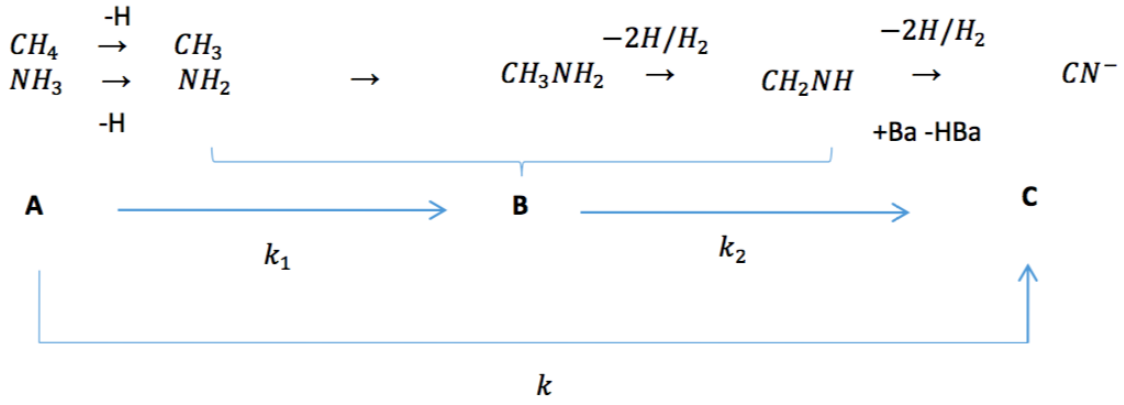


Figure 3.5: The formation mechanism of $CN^-$ proposed by Kim and Kaiser(2011).

during our warm-up phase. The ion fragment with m/z=31 is assigned as $CH_3NH_2^+$ and detectable in all ratios of our $CH_4$+$NH_3$ experiments (figure 3.6).

By the deviation performed in section 2.4, we have a rate equation for consecutive reactions 2.10. With one of the reactant larger than another, we applied the pseudo first order assumption. With equation 2.10, we fitted the formation of $CN^-$ (figure 3.7)and found that one of the rate constant is always larger than the other in all of the ratios. The fitting results are averaged by more than two experiments and are shown in table 3.4.The results of Kim and Kaiser is also listed into the table, they could observe a two-step reaction mechanism in production of $CN^-$ in $CH_4$+$NH_3$ (3:1) experiments with electron current 0.1 $\mu$A. However, when they increased the electron flux to 1 $\mu$A for irradiation $C_nH_{2n+2(n=1-6)}$ and $NH_3$ ice mixtures, they also observed a one-step reaction mechanism.

Table 3.4: The fitting results of $CN^-$ by equation 2.10

| Ratio of $CH_4$+$NH_3$ | A (x$10^{16}$ molecules cm$^{-2}$) | $k_1$ (x$10^{-18}$ photon$^{-1}$) | $k_2$ (photon$^{-1}$) |
|---|---|---|---|
| 1:20 | 4.75 ± 0.40 | 0.70 ± 0.09 | >1 |
| 1:10 | 4.51 ± 0.18 | 1.33 ± 0.13 | >1 |
| 1:5 | 4.61 ± 0.18 | 1.93 ± 0.19 | >1 |
| 3:2 | 2.24 ± 0.03 | 8.21 ± 0.70 | >1 |

A represents the amount of $CN^-$ we may obtain when irradiated the ice for infinitely long.

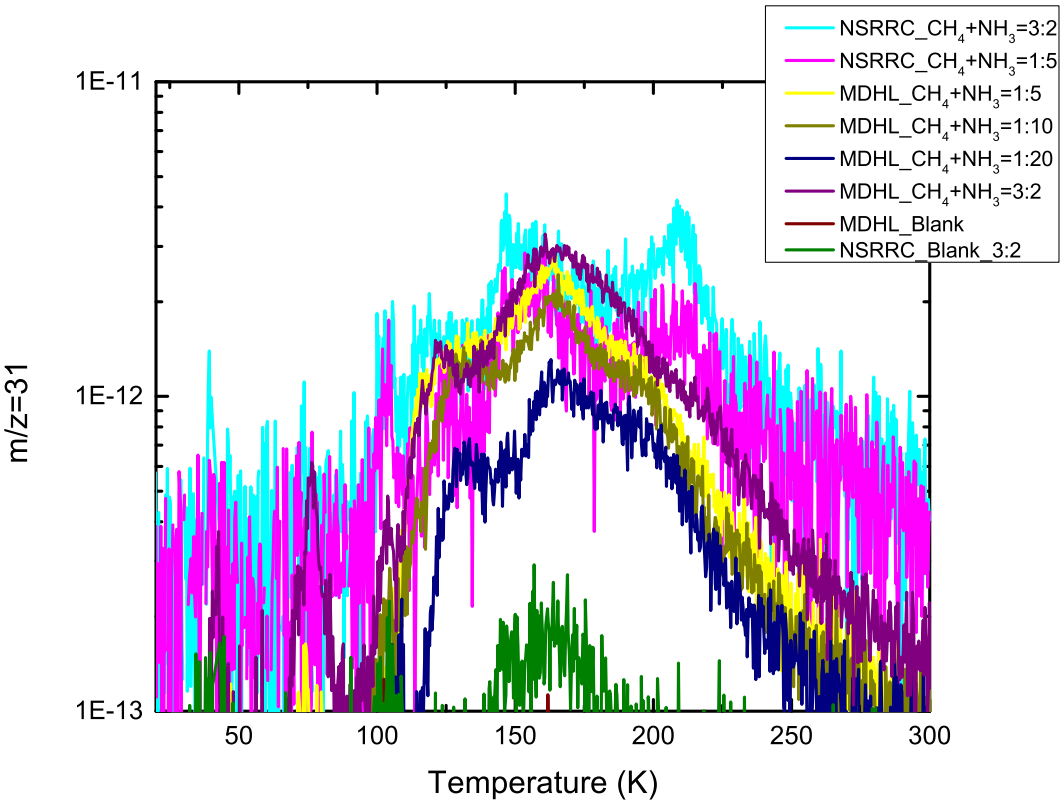


Figure 3.6: The m/z=31 detected by QMS during warm-up with heating rate 1 K/min in different configurations of ice mixtures.

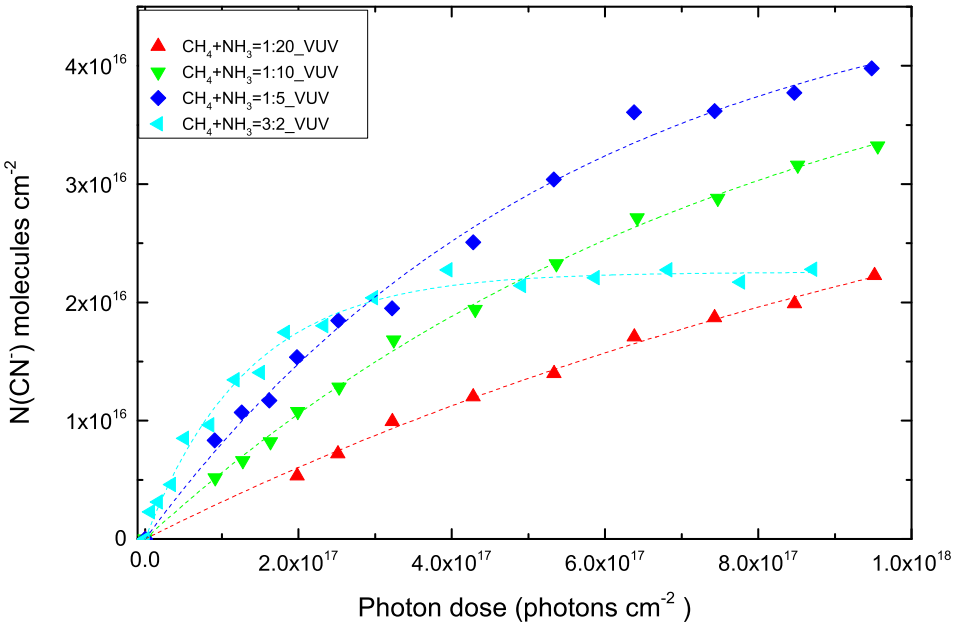


Figure 3.7: The column density of $CN^-$ accumulated when different configurations of $CH_4$ + $NH_3$ ice mixtures are irradiated by VUV photons provided by MDHL. The dotted lines are fits of column densities by equation 2.10.

## 3.3 The Concentration Effect in formation of Cyanide ions and Ethane

### 3.3.1 Cyanide ion

From table 3.4, we may observe that the rate $k_1$ is nearly proportional to the concentration of $CH_4$. As $CH_4$ to $NH_3$ ratio increases, more $CH_4$ are involved in $CH_3$ radical formation, thus there are more $CH_3$ radicals to produce $CH_3NH_2$ intermediates.

In $CH_4$ to $NH_3$ =3:2 ice mixtures, A is about half of that of the other ratios. The reduction is mainly because $NH_2$ (forming $CH_3NH_2$) has a competing relationship with $CH_2$, $CH_3$ and $C_2H_4$ radicals (forming $C_2H_6$ and $C_3H_8$). This competition supresses the production of intermediate $CH_3NH_2$, thus the formation of $CN^-$. Therefore, the yield of $CN^-$ is the least in $CH_4$ to $NH_3$ ice mixture with ratio 3:2 while the yield of $C_2H_6$ is the greatest in the mixture with the same ratio(table 3.4), (table 3.3)

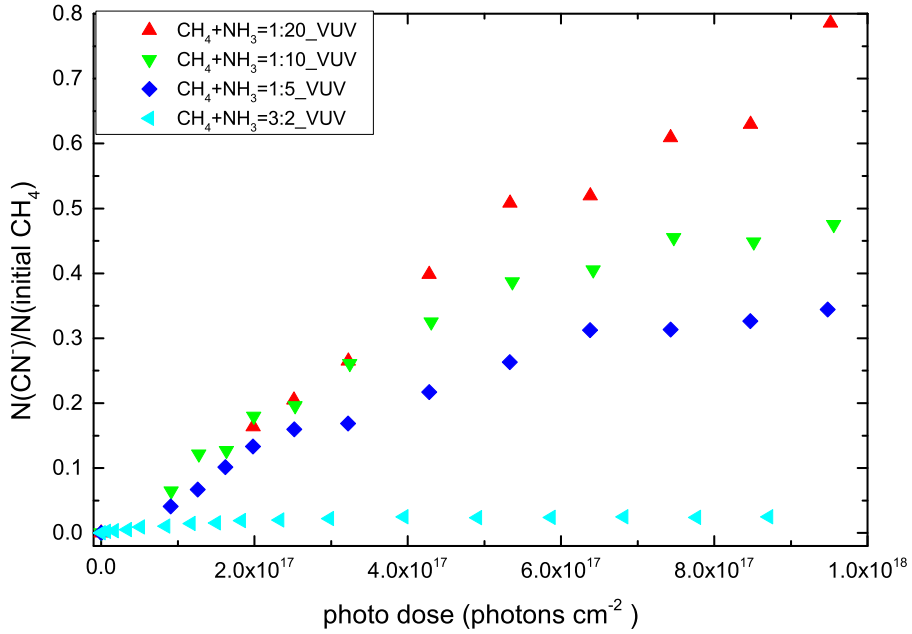


Figure 3.8: The column density of $CN^-$ divided by initial $CH_4$ accumulated when different configurations of $CH_4$ + $NH_3$ ice mixtures are irradiated by VUV photons provided by MDHL.

Considering the normalized $CN^-$ with respect to the initial $CH_4$(figure 3.8), the formation of $CN^-$ is more efficient in low $CH_4$ concentration ice mixtures. At low $CH_4$ concentration, there are excess $NH_3$ which can aggregate mobile $CH_3$ radicals, preventing meeting another $CH_3$ radical or $C_2H_4$. Therefore the production of $C_2H_6$ is greatly suppressed and more $CN^-$ will be produced.

### 3.3.2 Ethane

Considering the case of ratio of $CN^-$ divided by $C_2H_6$,the formation of $CN^-$ in ice mixtures with diluted $CH_4$ has more $CN^-$ formed then $C_2H_6$. It is because ice mixtures with with higher concentrations in $CH_4$ is more effective for one $CH_3$ radical to combine with another $CH_3$ radical. On the contrast, $CH_3$ radicals formed in the ice mixtures with diluted $CH_4$ concentrations are aggregated by $NH_3$. Therefore, $CN^-$ is less efficient to form in ice mixtures with excess $NH_3$.

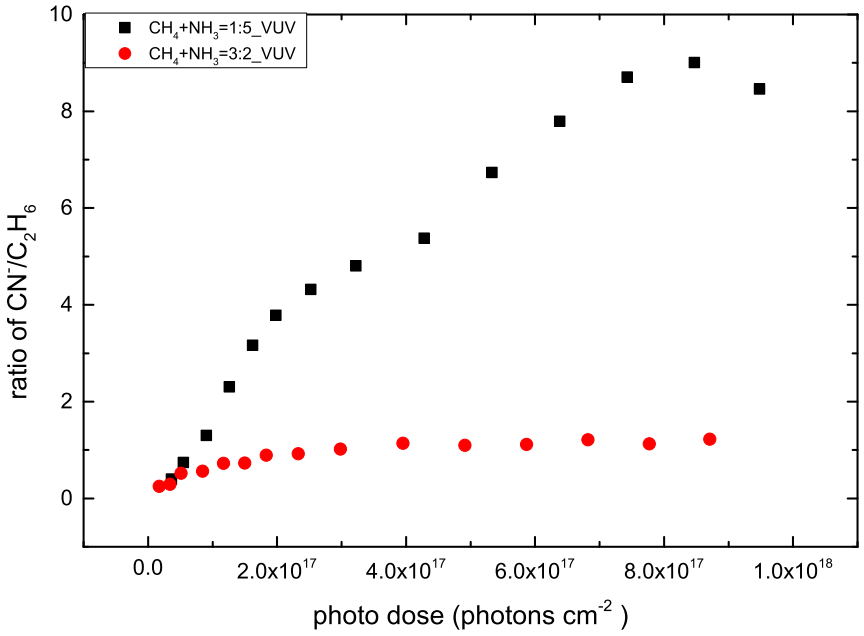


Figure 3.9: The column density of $CN^-$ divided by $C_2H_6$ accumulated when different configurations of $CH_4$ + $NH_3$ ice mixtures are irradiated by VUV photons provided by MDHL.

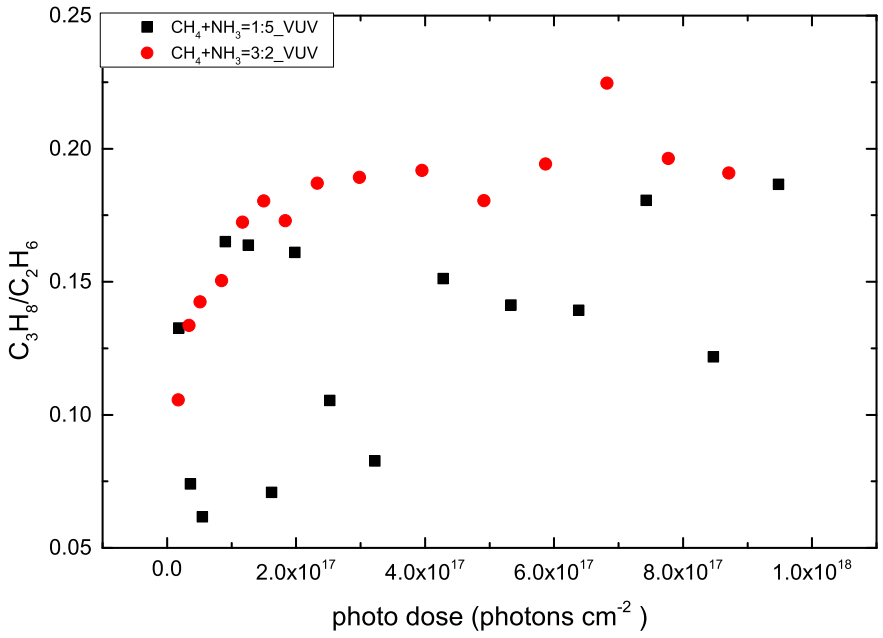


Figure 3.10: The column density of $C_3H_8$ divided by $C_2H_6$ accumulated when different configurations of $CH_4$ + $NH_3$ ice mixtures are irradiated by VUV photons provided by MDHL.

### 3.3.3 Propane

$C_3H_8$ forms based on to the $C_2H_6$ 3.10 is the plot with column densities of $C_2H_6$ divided by $C_3H_8$. We may see that the ratio in $CH_4$+$NH_3$ =1:5 experiment is around 6 where $CH_4$+$NH_3$ =3:2 is around 3. This shows that the amount of $C_3H_8$ in $CH_4$+$NH_3$ =3:2 experiment is higher. It is rather difficult for $C_3H_8$ to form in $CH_4$+$NH_3$ = 1:5 experiments because $NH_3$ aggregated them. The formation of $C_3H_8$ in CH4+NH3 =1:5 and 3:2 experiments has given a reasonable explanation about why $C_2H_6$ formation is most efficient in $CH_4$+$NH_3$ =1:10 experiments.

## 3.4 Photon Energy Effect - EUV and VUV

According to Blanksby and Ellison [23], the dissociation energy for $CH_4$, becoming $CH_3$, $CH_2$ CH and C are 4.55, 4.79, 4.39 and 3.51 eV respectively at 298 K. Whereas dissociation energy for $NH_3$, becoming $NH_2$ is 4.67 eV at 298 K.

Considering our MDHL with average energy of 9.27 eV, all of the above fragments may exist either in the form of radicals or combined with other radicals to form heavier molecules in our ice mixtures. Although Increasing the photon energy does not create new fragmentation pathway, the choice of fragmentation pathways depends on photon energy.

Several gaseous state measurements also support this statement. First, Gans et al. (2011) [24] changed VUV photon wavelengths from 121.6 nm to 118.2 nm to dissociate the $CH_4$ molecules and ionize the fragments with the corresponding photon energy. Changing the output of the pulsed laser from 121.6 to 118.1 nm significantly changed the ratio of $CH_3^+$ and $CH_2^+$, produced from fragmentation, from 1: 1 to 1:2. This slight change of photon energy, from 10.2 eV to 10.4 eV has a significant change in the ratio between different pathways.

Second, an EUV fragmentation experiment done by Tsai et al. [25] used 30.4 nm to photo-dissociate $CH_4$ and tested it by timeĂŞ - of ĂŞ-flight mass spectrometer yields $CH_3^+$: $CH_2^+$: $CH^+$: $C^+$ = 1 :0.32: 0.118: 0.0237 (Tsai 1980). Consider the ratios of $CH_3$ to $CH_2$ radicals, it is around 3 to 1, which is in contrast to the experiment results of Gans et

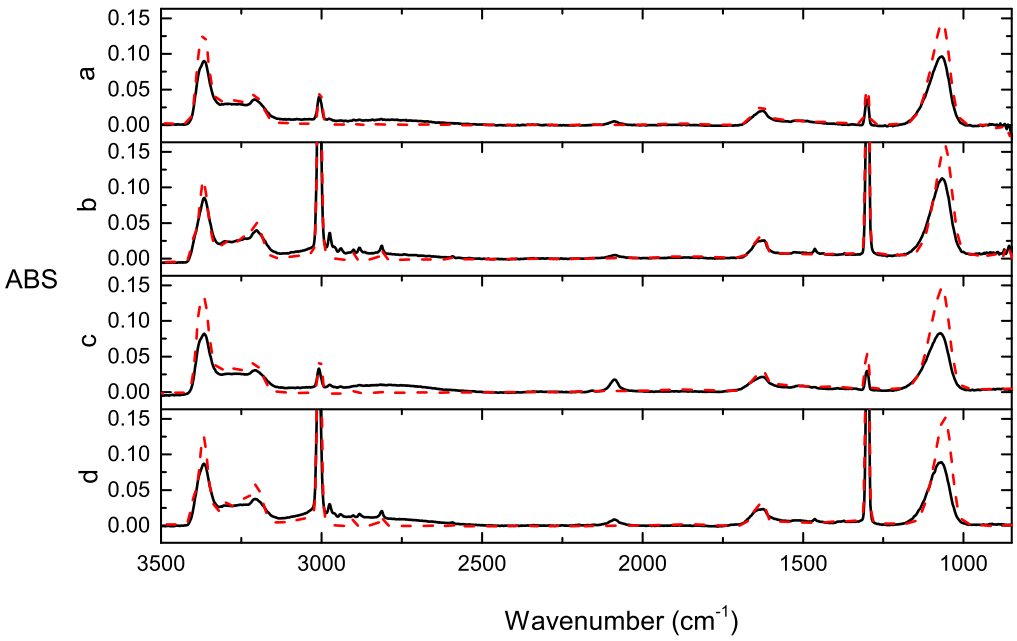


Figure 3.11: The the infra-red spectrum of $CH_4$ + $NH_3$ ice mixtures before irradiation (dashed) and VUV and EUV (solid) irradiated ice mixtures provided by MDHL. (a) and (b) are EUV irradiated $CH_4$+$NH_3$ = 1:5 and 3:2 ice mixtures respectively, and (c) and (d) are VUV irradiated $CH_4$+$NH_3$ = 1:5 and 3:2 ice mixtures respectively.

al. (2011)[24]. Although both of them are gaseous state experimental results, it is uncertain that if increasing photon energy can produce more $CH_2$ radicals.

Thirdly, a group varies ratios of $CH_4$ + $NH_3$ mixtures and irradiate with far UV irradiation at 134 nm [26]. However, this group only used gas chromatography to analyse the final products and their reaction is carried in gas phase in room temperature. We aware that the VUV absorption spectra of $CH_4$ in solid phases is different from gaseous phases [27], so the exact photo dissociation fragmentation ratios by EUV nor VUV irradiations in astronomical environments are still unknown. It is worthwhile for us to perform the experiment by EUV irradiation to see if EUV irradiation can generate any new products on the surface of Charon, or any difference in yield. Despite the photon energy of our MDHL is enough to dissociate both the $CH_4$ and $NH_3$ molecules, we further increase photon energy to He II 30.4 nm to examine the differences in photo-products.

Table 3.5 shows the identified peaks of $CH_4$+$NH_3$ ice mixtures irradiated by VUV and EUV (30.4 nm) irradiated in IR spectra (figure 3.11).

Table 3.5: The peak positions of identified substances after VUV and EUV irradiations in different configurations of ice mixtures.

| Literture assignments | | $CH_4$+$NH_3$ ratio (MDHL) | | $CH_4$+$NH_3$ ratio (30.4 nm) | | |
|---|---|---|---|---|---|---|
| Wavenumber ($cm^{-1}$) | Carrier | 1:5 ($cm^{-1}$) | 3:2 ($cm^{-1}$) | 1:5 ($cm^{-1}$) | 3:2 ($cm^{-1}$) | Ref. |
| 3375 | $\nu_3$ ($NH_3$) | 3366 | 3367 | 3368 | 3368 | 1 |
| 3290 | $2\nu_4$ ($NH_3$) | - | - | - | - | 1 |
| 3210 | $\nu_1$ ($NH_3$) | 3207 | 3205 | 3209 | 3205 | 1 |
| 3011 | $\nu_3$ ($CH_4$) | - | - | - | - | 2 |
| 2972 | $\nu_{10}$ ($C_2H_6$) | 2975 | 2975 2977 | 2976 | | 3 |
| 2960 | $C_3H_8$ | - | 2960 | - | 2960 | 7 |
| 2941 | $\nu_8 + \nu_1 1$ ($C_2H_6$) | 2940 | 2940 | - | 2942 | 3 |
| 2904 | $\nu_1$ ($CH_4$) | 2901 | 2901 | 2901 | 2901 | 5 |
| 2879 | $\nu_5$ ($C_2H_6$) | 2882 | 2882 | - | 2884 | 3 |
| 2814 | $\nu_2 + \nu_4$ ($CH_4$) | - | 2815 | - | 2813 | 5 |
| 2083 | $\nu$ ($CN^-$) | 2088 | 2088 | 2090 | 2089 | 2 |
| 1625 | $\nu_4$ ($NH_3$) | 1625 | 1631 | 1627 | 1631 | 1 |
| 1514 | $\delta$ ($NH_2$) | 1509 | 1511 | 1509 | 1511 | 6 |
| 1465-1440 | deform $CH_2$ scissor | 1461 | 1463 | - | 1465 | 3,4 |
| 1390-1370 | $CH_3$ sym deform | 1394 | 1372 | - | 1372 | 4 |
| 1298 | $\nu_4$ ($CH_4$) | 1301 | 1299 | 1303 | 1301 | 2 |
| 1075 | $\nu_2$ ($NH_3$) | 1073 | 1072 | 1070 | 1068 | 1 |
| 820 | $\nu_1 2$ ($C_2H_6$) | - | 820 | - | - | 3 |

Reference: 1. Bossa et al. 2008 [9] 2. Moore and Hudson 2003 [10] 3. Kim et al. 2010 [11] 4. Socrates 2001 [12] 5. Bennet and Kaiser 2007 [13] 6. Zheng et al. 2008 [14] 7. Hudson and Moore 2004 [15]

Considering the formation mechanisms of $C_2H_6$ and $C_3H_8$, equation (3.2 and 3.4), when MDHL VUV irradiation is replaced by He II 30.4 nm monochromatic light, the ratio of $C_2H_6$ to $C_3H_8$ in $CH_4$ to $NH_3$ = 3:2 ice mixtures irradiated by VUV irradiation is lower under EUV irradiation than that under EUV provided by NSRRC (figure 3.12). There are two possible explanations. First, different photon energies flavour different $CH_4$ fragmentation pathway and less $C_3H_8$ is produced with EUV photons. Second, the efficiency of $CH_4$ fragmentation is greatly reduced under EUV irradiation and the density of $CH_3$ radicals are much lower than that in the case of VUV irradiation provided by the MDHL. We lengthen the time of EUV irradiation on our ice mixtures until the total number of destructed $CH_4$ is similar to that in VUV irradiation experiments done with MDHL. The averages of ratios of $C_2H_6$:$C_3H_8$ of the last 7 irradiations before terminating irradiations are 3.53 in VUV and

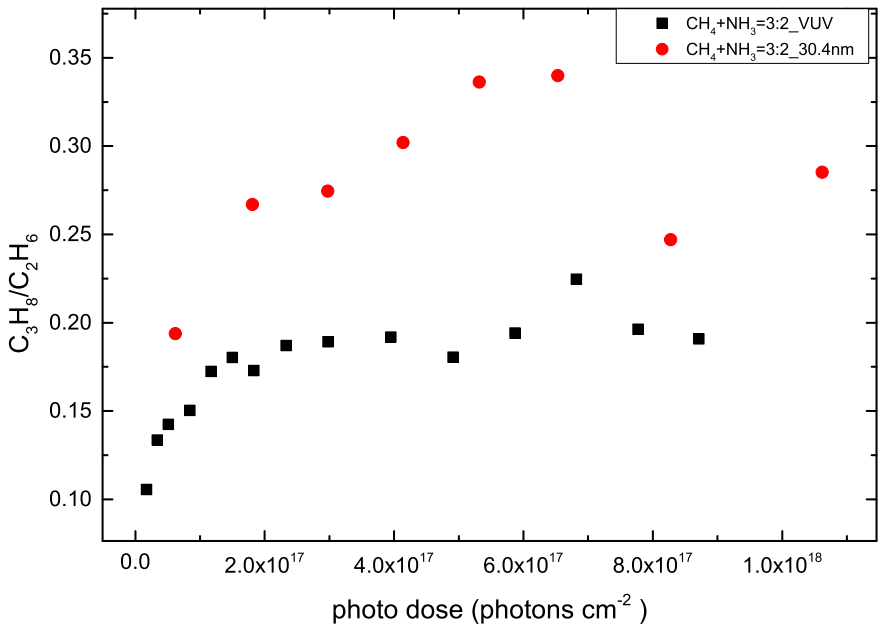


Figure 3.12: The column density of $C_3H_8$ divided by $C_2H_6$ accumulated when different configurations of $CH_4$ + $NH_3$ ice mixtures are irradiated by VUV and EUV photons

3.66 in EUV. The result supports the latter explanation. From figure 3.13, The reduction of $CH_4$ is 6.06± times slower in EUV experiments than VUV experiments while the reduction of $NH_3$ is 3.19±0.12 times lower. Therefore, the destruction cross-section of $CH_4$ and $NH_3$ ice has a 6.06±0.07 and 3.19±0.12 times lower in 30.4 nm than in 121.6 nm.

Figure 3.12 shows the column densities of $C_2H_6$ divided by $C_3H_8$ after $CH_4$ + $NH_3$ =3:2 ice mixtures are irradiated by VUV irradiation and He II monochromatic light.

From 3.12, we may observe that more $C_3H_8$ is produced by 30.4nm photons than by VUV photons. Recall the formation mechanism of $C_3H_8$ (equation 3.5), $CH_2$ and $C_2H_4$ radicals are esccential in producing $C_3H_8$. This increase production in $C_3H_8$ may be caused by the increase in $CH_2$ radicals during fragmentation of $CH_4$. This result is similar to the findings of Gans et al. (2011)[24], the ratio of $CH_2$ radicals increases from 0.3 to 0.48 when photon energy increases from 121.6 nm to 118.2 nm in their pulsed laser experiments.

Apart from $C_2H_6$ and $C_3H_8$, are there any difference in $CN^-$ pro-

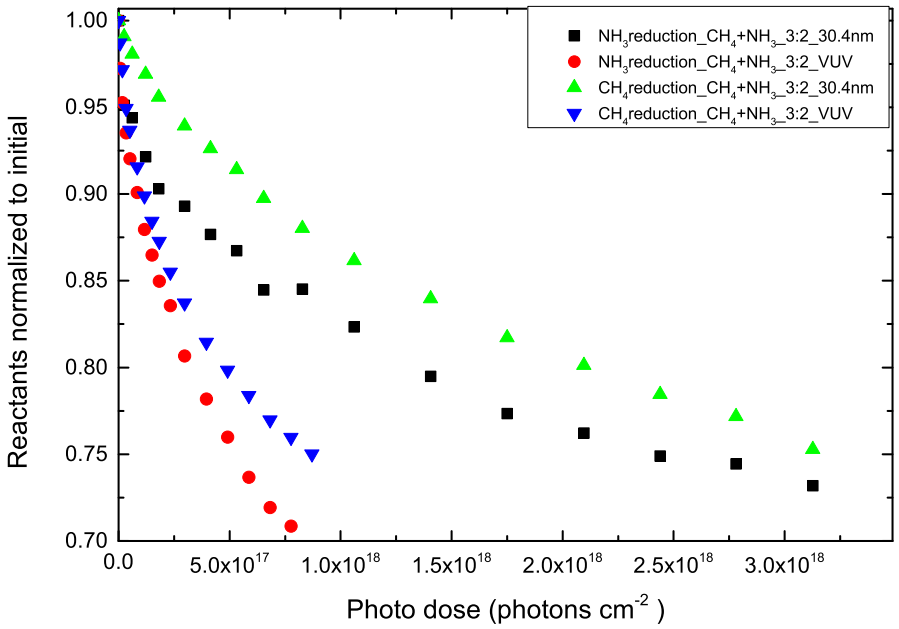


Figure 3.13: The normalized reduction of $CH_4$ and $NH_3$ in $CH_4$ + $NH_3$ ice mixtures irradiated by VUV and EUV photons

duction? Figure 3.14 shows the accumulated column densities of $CN^-$ generated by irradiation of $CH_4$+$NH_3$ ice mixtures by MDHL and 30.4 nm monochromatic light. The fitting results are shown in Table 3.6. The rate constants forming $CN^-$ is 3.06 to 4.13 times larger in $CH_4$+$NH_3$ = 1:5 and 3:2 irradiated by MDHL than irradiated by 30.4 nm monochromatic light respectively. From figure 3.13, the destruction cross-section of $CH_4$ and $NH_3$ are reduced by 6.06±0.07 and 3.19±0.12 times respectively. The formation rate constants of $CN^-$ is 3.06 to 4.13 times smaller than VUV irradiations (table **??**. Therefore, we may conclude that the reduction in $CN^-$ formation rate by 30.4nm EUV irradiation is mainly due to the decreased $NH_3$ destruction cross-sections.

## 3.5 Residues

The residues we studied are the accumulated residues onto the substrate. We do not understand are there any interaction between residues and the ice mixtures. However, we may know what is the change of residues when we change the ratio of the $CH_4$+$NH_3$ from $CH_4$ dominating to $NH_3$ dominating. Figure 3.15 is a comparison of $CH_4$+$NH_3$ =

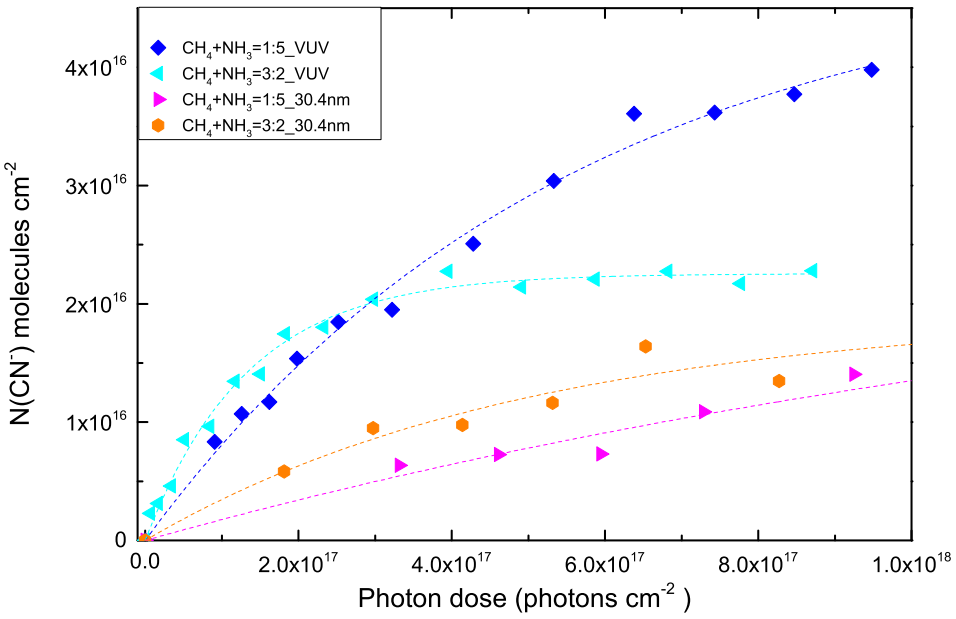


Figure 3.14: The column densities of $CN^-$ generated by irradiation of $CH_4$+$NH_3$ ice mixtures by MDHL and 30.4 nm monochromatic light.

Table 3.6: The fitting results of $CN^-$ by equation 2.10

| Light source | Ratio of $CH_4$+$NH_3$ | A (x$10^{16}$ molecules $cm^{-2}$) | $k_1$ (x$10^{-18}$ $photon^{-1}$) | $k_2$ ($photon^{-1}$) |
|---|---|---|---|---|
| VUV | 1:5 | 4.61 ± 0.18 | 1.93 ± 0.19 | >1 |
| MDHL | 3:2 | 2.24 ± 0.03 | 8.21 ± 0.70 | >1 |
| EUV | 1:5 | 2.89 ± 1.29 | 0.63 ± 0.37 | >1 |
| 30.4nm | 3:2 | 2.24 ± 0.03 | 1.92 ± 1.99 | >1 |

Fitting result of figure 3.14 with pseudo first order equation $[CN^-]=A(1-e^{-kx})$. These fitting results of MDHL experiments are an average of at least 2 experiments with the same circumstances. In the expression, A represents the column density when x, the photon dose, becomes infinitely large and k is the rate constant.

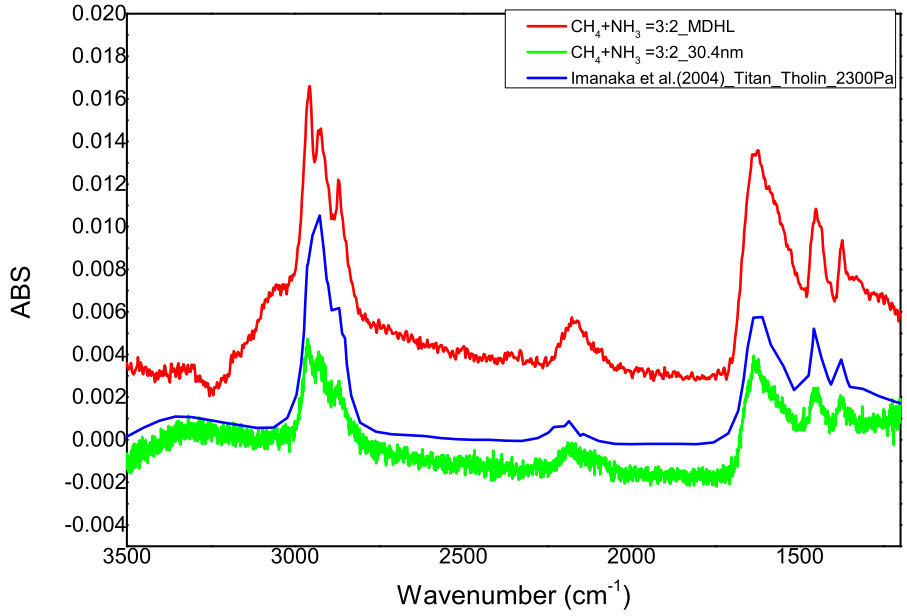


Figure 3.15: The IR spectrum of residues in after $CH_4$+$NH_3$ = 3:2 experiments and the accumulate residues after MDHL experiments and NSRRC experiments.

3:2 after VUV experiments, residues accumulated after EUV exposure of $CH_4$ + $NH_3$ = 3:2 ice mixtures and the plasma experiment done by Imanaka et al. (2004)[8]. The residues in ammonia dominated ice mixtures cannot be detected after consecutive experiments. There are no differences between EUV accumulated residues and VUV accumulated residues in $CH_4$+$NH_3$ = 3:2 ice mixtues. The main differences between plasma experiments of $N_2$+$CH_4$ (9:1) done at 2300 Pa. by Imanaka et al. (2004)[8] and our experiments is the peaks located around 2090 $cm^{-1}$.

Why we use different initial reactants, replacing $N_2$ by $NH_3$ but we may get similar residues? The similarities during formation of atomic nitrogens when breaking $N_2$ bonds in nitrogen and NH bonds in ammonia give rise to this result. When photon energy is enough to break both NH bond and $N_2$ bond, similar experimental residues forms. Our results implies that the residues formed on Charon is similar to what we found on Titan, although their formation environments differs from gaseous phase with $N_2$ dominating to solid phase with $NH_3$.

## 3.6 Conclusion

The main product of VUV and EUV irradiated $CH_4$+$NH_3$ ice mixtures are $C_2H_6$ and $CN^-$. $C_3H_8$ is also produced by $C_2H_6$ or $C_2H_2$. We did several investigations towards $CH_4$+$NH_3$ ice mixtures. First, by changing ratio of $CH_4$ and $NH_3$ in the ice mixture, $CN^-$ production is more effective in $NH_3$ dominated ice mixtures where $C_2H_6$ dominates in $CH_4$ dominated ice mixtures. Second, by changing the photon source to EUV irradiation, the yield of $C_3H_8$ increases. The effective formation of $C_3H_8$ was not produced by $C_2H_6$ but by $C_2H_2$ and $CH_4$ because the ratio of $C_3H_8$ : $C_2H_6$ increases. This suggests that the $CH_2$ or CH fragmentation from $CH_4$ increases when photon energy increases. By studying the production efficiencies, the difference in photo-production yield is mainly caused by the reduction in photo-destruction cross-section in the reactants. Thirdly, by comparison with electron irradiation experiments, electron irradiation has a smaller absorption cross-sections, the percentage of yield is also smaller than VUV irradiated ice mixtures with similar ice thicknesses. Finally, we compared our residues obtained with laboratory produced Taitan tholins, the similar infra-red spectrum shows a similar functional groups in residues. Our result implies that the tholin on Charon should be similar to the tholin formed on Titan.


國立中央大學

# 4. Astrophysical Implications

The main source to irradiating the dark side of Charon is Ly$\alpha$ reflected by interplanetary medium [1]. Other sources included energetic ions in solar wind, which mainly consist of $H^+$, $He^+$, $He^{++}$ and $O^{2+}$ etc. originated from solar corona or IPM. These ions also reflect solar irradiation to the dark side of Charon. Among sources focused on He II irradiation as it is 3 to 20 times more intense than He I during a solar flare. As the intensity varies with solar activities, it is difficult to estimate the dose onto Charon. Besides, electronic flux is also present in solar wind, the flux for energetic electrons observed at the 1 A. U. position is available (http://www.swpc.noaa.gov/products/goes-electron-flux).

In this chapter, we will discuss the effects of three difference energy sources , including EUV, VUV and energetic (5 keV) electrons on production of cyanide ions and their implication on Charon. First, we compare the destructive cross-sections of these sources, and then their corresponding production yields in $CN^-$.

## 4.1 The reduction of methane and ammonia by photon sources and electrons

In electron irradiation experiments of Kim and Kaiser (2011)[22], the energy transferred to $CH_4$ + $NH_3$ ice mixtures is by linear electron transfer (LET) of 3.1 keV $\mu m^{-1}$, in the order of magnitude of the MeV cosmic rays typically transferred to the ice samples. Their dose reached 1.3 eV molecule$^{-1}$ in 90 minutes with about 610 ML of $CH_4$ and 260 ML of $NH_3$.

The percentage of photons absorbed by $CH_4$ and $NH_3$ ice mixtures under VUV irradiation is calculated by substituting cross-sections measured by Cruz-Diaz et al. [27] and the VUV intensity spectrum of our MDHL into Beer′s law. $CH_4$+$NH_3$ = 3:2 ice mixtures can absorb more

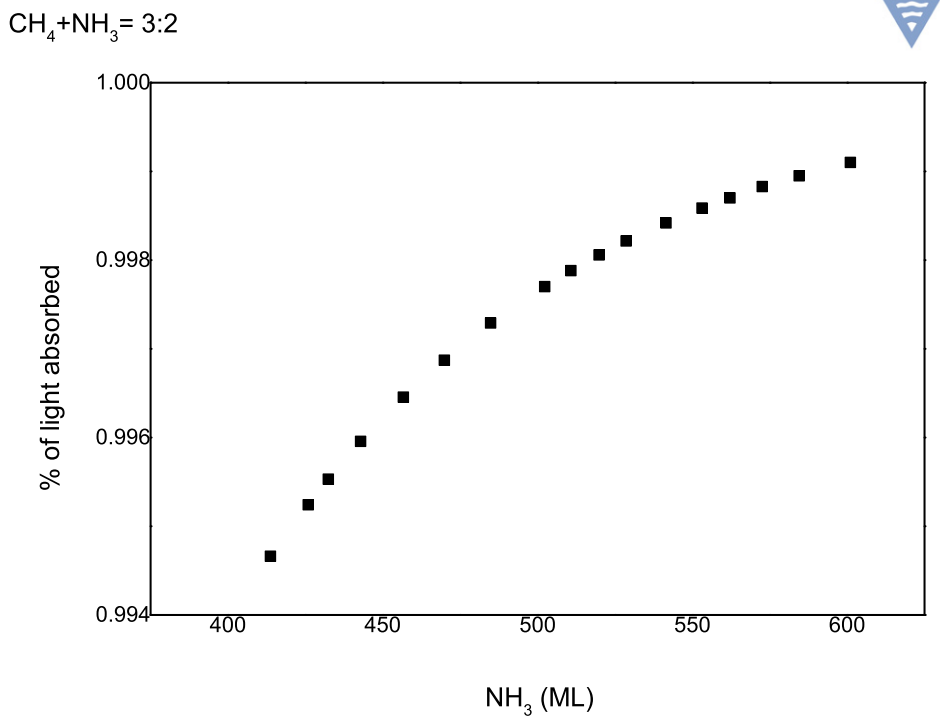


Figure 4.1: The calculated percentage of VUV irradiation absorbed by different thickness of $CH_4$ to $NH_3$ = 3:2 ice mixtures.

than 99 % of light when thickness of $NH_3$ equals 600 ML (figure

Regarding EUV irradiations, since there are no suitable windows (used for cutting off higher order lights) to measure the absorption of ices, it is impossible to obtain absorption cross-sections right now. From figure 3.13, we obtained the distructive cross-sections of EUV to VUV photons. The $CH_4$ reduction by EUV photons is 6.06±0.07 times lower than VUV irradiation. From the New Horizons Mission, EUV irradiation (>12.4 eV) is $8.7 \times 10^7 eV cm^{-2} s^{-1}$ at mean heliocentric distance (39 A.U.) of Charon whereas VUV irradiation (Ly-$\alpha$) is $1.9 \times 10^9 eV cm^{-2} s^{-1}$[1]. Since VUV flux is one order of magnitude more intense then EUV fluxes and the $CH_4$ reduction is about 6 times higher than EUV irradiation, it is the main source participants the reduction of $CH_4$.

## 4.2 Cyanide ion produced by photon sources and electrons

Considering the ice mixtures in which $CH_4$ is dominated, the efficiencies in $CN^-$ formation by electrons and VUV irradiations is calcu-

lated by the final column densities divided by the column densities of the limiting reactant. A fixed amount of $CN^-$ is obtained after irradiations. In our MDHL experiments, we have 14.8 ML of $CN^-$ obtained in ($CH_4$ = 900 ML, $NH_3$= 600 ML) ice mixtures. Kim and Kaiser (2011) irradiated ice mixtures($CH_4$ = 610 ML, $NH_3$= 260 ML) and obtained 13 - 16 ML of $CN^-$ adopting the $CN^-$ absorption coefficient ($3.7 \times 10^{-18}$ cm molecule$^{-1}$) [28], which is 4.86 times smaller than the absorption strength we adopted. We do not adopt the same absorption coefficient because the number of $CN^-$ produced will exceed $CH_4$ consumption. If we adopted the same absorption coefficient, the production yield of $CN^-$ should be multiplied by 4.86. Therefore, our yield is 72 ML of $CN^-$. Regarding percentage of $NH_3$ (limiting reactant), Kim and Kaiser has 5 - 6 % yield where we have 12 % yield if we adopted the same absorption coefficients.

The above situation is ideal to apply on the slow depositing ices or very thick ices, where photons or electrons can irradiate the surface without renewal. For fast depositing ices, this case is not suitable because only the first few layers are irradiated (figure 4.1). The depositing (hitting) rates of $CH_4$ onto the surface of Charon, shown in figure **??**, varies from 2 to 6 $\times$ $10^{11}$ $m^{-2}$ $s^{-1}$ due to the tidal locked rotation of Pluto and charon. In 1 pluto winter (130 earth years), around 110 ML of $CH_4$ will be deposited onto the pole positions, and 3 times more abundant than that at the pole positions facing pluto. This deposition rate is a slow depositing ice because from our experiments: figure 3.14, after $4 \times 10^{17}$ VUV photons (about 1 Pluto year), maximum $CN^-$ is formed.

As a result, under winter time, If we only consider VUV photon source, assuming ratio of $CH_4$ to $NH_3$ is 3:2, about 15 ML of $CN^-$ will be formed during winter time, leading to similar residues as Titan.

## 4.3 Conclusion

Through investigating methane($CH_4$) and ammonia($NH_3$) ice mixtures, we better understand the followings relations: 1. The formation yield of cyanide ion ($CN^-$) is not proportional to the initial deposited methane when methane is dominating. However, the formation rate is proportional to its initial $CH_4$ to $NH_3$ ratios. The competition between

$CH_3$ radicals (forming both $CH_3NH_2$ and $C_2H_6$) and $NH_2$ radicals (forming $CH_3NH_2$) results the former result. 2. When VUV is replaced by 40.8 eV 30.4nm He II EUV irradiations, the destruction cross-section of $CH_4$ and $NH_3$ are reduced by 6.06±0.07 and 3.19±0.12 times respectively. The lower formation rate of $CN^-$ in EUV irradiation by 3.06 to 4.13 times is mainly due to the reduced $NH_3$ destruction cross-sections. 3. The photo fragmentation of $CH_4$ by more energetic photons are more likely to form $C_3H_8$ than $C_2H_6$, may infer there are new reaction mechanism pathways (with higher energy barrier) involved to produce $C_3H_8$. 4. The functional groups of residues obtained in $CH_4$ to $NH_3$ = 3:2 ice mixtures are similar to the laboratory made Titan tholins.

# Bibliography


[1] W. Grundy, D. Cruikshank, G. Gladstone, C. Howett, T. Lauer, J. Spencer, M. Summers, M. Buie, A. Earle, K. Ennico *et al.*, "The formation of charon's red poles from seasonally cold-trapped volatiles," *Nature*, vol. 539, no. 7627, pp. 65–68, 2016.

[2] W. Grundy, R. Binzel, B. Buratti, J. Cook, D. Cruikshank, C. Dalle Ore, A. Earle, K. Ennico, C. Howett, A. Lunsford *et al.*, "Surface compositions across pluto and charon," *Science*, vol. 351, no. 6279, p. aad9189, 2016.

[3] W. A. Hoey, S. K. Yeoh, L. M. Trafton, D. B. Goldstein, and P. L. Varghese, "Rarefied gas dynamic simulation of transfer and escape in the pluto–charon system," *Icarus*, no. 287, pp. 87–102, 2017.

[4] J. C. Cook, S. J. Desch, T. L. Roush, C. A. Trujillo, and T. Geballe, "Near-infrared spectroscopy of charon: Possible evidence for cryovolcanism on kuiper belt objects," *The Astrophysical Journal*, vol. 663, no. 2, p. 1406, 2007.

[5] G. R. Gladstone, W. R. Pryor, and S. A. Stern, "Ly$\alpha$@ pluto," *Icarus*, vol. 246, pp. 279–284, 2015.

[6] Y.-J. Chen, K.-J. Chuang, G. M. Caro, M. Nuevo, C.-C. Chu, T.-S. Yih, W.-H. Ip, and C.-Y. Wu, "Vacuum ultraviolet emission spectrum measurement of a microwave-discharge hydrogen-flow lamp in several configurations: application to photodesorption of co ice," *The Astrophysical Journal*, vol. 781, no. 1, p. 15, 2013.

[7] T.-F. Hsieh, L.-R. Huang, S.-C. Chung, T.-E. Dann, P.-C. Tseng, C. Chen, and K.-L. Tsang, "Design of a high-flux and high-resolution vuv bending-magnet beamline," *Journal of synchrotron radiation*, vol. 5, no. 3, pp. 562–564, 1998.

[8] H. Imanaka, B. N. Khare, J. E. Elsila, E. L. Bakes, C. P. McKay, D. P. Cruikshank, S. Sugita, T. Matsui, and R. N. Zare, "Laboratory experiments of titan tholin formed in cold plasma at various pressures: implications for nitrogen-containing polycyclic aromatic compounds in titan haze," *Icarus*, vol. 168, no. 2, pp. 344–366, 2004.

[9] J.-B. Bossa, P. Theulé, F. Duvernay, F. Borget, and T. Chiavassa, "Carbamic acid and carbamate formation in $nh_3$+$co_2$ ices–uv irradiation versus thermal processes," *Astronomy & Astrophysics*, vol. 492, no. 3, pp. 719–724, 2008.

[10] M. Moore and R. Hudson, "Infrared study of ion-irradiated n 2-dominated ices relevant to triton and pluto: Formation of hcn and hnc," *Icarus*, vol. 161, no. 2, pp. 486–500, 2003.

[11] Y. Kim and R. Kaiser, "Abiotic formation of carboxylic acids (rcooh) in interstellar and solar system model ices," *The Astrophysical Journal*, vol. 725, no. 1, p. 1002, 2010.

[12] G. Socrates, "Infrared and raman characteristic group frequencies, 3rd," 2001.

[13] C. J. Bennett and R. I. Kaiser, "The formation of acetic acid (ch3cooh) in interstellar ice analogs," *The Astrophysical Journal*, vol. 660, no. 2, p. 1289, 2007.

[14] W. Zheng, D. Jewitt, Y. Osamura, and R. I. Kaiser, "Formation of nitrogen and hydrogen-bearing molecules in solid ammonia and implications for solar system and interstellar ices," *The Astrophysical Journal*, vol. 674, no. 2, p. 1242, 2008.

[15] R. Hudson and M. Moore, "Reactions of nitriles in ices relevant to titan, comets, and the interstellar medium: formation of cyanate ion, ketenimines, and isonitriles," *Icarus*, vol. 172, no. 2, pp. 466–478, 2004.

[16] C. R. Richey and P. Gerakines, "Near-infrared band strengths of molecules diluted in n2 and h2o ice mixtures relevant to interstellar and planetary ices," *The Astrophysical Journal*, vol. 759, no. 1, p. 74, 2012.

[17] L. d'Hendecourt and L. Allamandola, "Time dependent chemistry in dense molecular clouds. iii-infrared band cross sections of molecules in the solid state at 10 k," *Astronomy and Astrophysics Supplement Series*, vol. 64, pp. 453–467, 1986.

[18] F. Borget, G. Danger, F. Duvernay, M. Chomat, V. Vinogradoff, P. Theulé, and T. Chiavassa, "Aminoacetonitrile characterization in astrophysical-like conditions," *Astronomy & Astrophysics*, vol. 541, p. A114, 2012.

[19] M. Moore and R. Hudson, "Infrared study of ion-irradiated water-ice mixtures with hydrocarbons relevant to comets," *Icarus*, vol. 135, no. 2, pp. 518–527, 1998.

[20] J. A. Noble, P. Theule, F. Borget, G. Danger, M. Chomat, F. Duvernay, F. Mispelaer, and T. Chiavassa, "The thermal reactivity of hcn and nh3 in interstellar ice analogues," *Monthly Notices of the Royal Astronomical Society*, vol. 428, no. 4, pp. 3262–3273, 2012.

[21] C. J. Bennett, C. S. Jamieson, Y. Osamura, and R. I. Kaiser, "Laboratory studies on the irradiation of methane in interstellar, cometary, and solar system ices," *The Astrophysical Journal*, vol. 653, no. 1, p. 792, 2006.

[22] Y. Kim and R. Kaiser, "on the formation of amines (rnh2) and the cyanide anion (cn–) in electron-irradiated ammonia-hydrocarbon interstellar model ices," *The Astrophysical Journal*, vol. 729, no. 1, p. 68, 2011.

[23] S. J. Blanksby and G. B. Ellison, "Bond dissociation energies of organic molecules," *Accounts of chemical research*, vol. 36, no. 4, pp. 255–263, 2003.

[24] B. Gans, S. Boyé-Péronne, M. Broquier, M. Delsaut, S. Douin, C. E. Fellows, P. Halvick, J.-C. Loison, R. R. Lucchese, and D. Gauyacq, "Photolysis of methane revisited at 121.6 nm and at 118.2 nm: quantum yields of the primary products, measured by mass spectrometry," *Physical Chemistry Chemical Physics*, vol. 13, no. 18, pp. 8140–8152, 2011.

[25] B. P. Tsai and J. H. Eland, "Mass spectra and doubly charged ions in photoionization at 30.4 nm and 58.4 nm," *International Journal of Mass Spectrometry and Ion Physics*, vol. 36, no. 2, pp. 143–165, 1980.

[26] A. Bossard and G. Toupance, "Far uv photolysis of ch4–nh3 mixtures and planetary studies," *Nature*, vol. 288, no. 5788, pp. 243–246, 1980.

[27] G. Cruz-Diaz, G. M. Caro, Y.-J. Chen, and T.-S. Yih, "Vacuum-uv spectroscopy of interstellar ice analogs-i. absorption cross-sections of polar-ice molecules," *Astronomy & Astrophysics*, vol. 562, p. A119, 2014.

[28] M. K. Georgieva and E. A. Velcheva, "Computational and experimental studies on the ir spectra and structure of the simplest nitriles (c1 and c2), their anions, and radicals," *International journal of quantum chemistry*, vol. 106, no. 6, pp. 1316–1322, 2006.